EFFECTS OF LARGE MODIFIERS IN AMORPHOUS MATERIALS USING TIME-DOMAIN TERAHERTZ SPECTROSCOPY

BY

THOMAS E. REIN

A THESIS
SUBMITTED TO THE FACULTY OF

ALFRED UNIVERSITY

IN PARTIAL FULFILLMENT OF THE REQUIREMENTS
FOR THE DEGREE OF

MASTER OF SCIENCE

IN

GLASS SCIENCE

ALFRED, NEW YORK
MARCH, 2014

EFFECTS OF LARGE MODIFIERS IN AMORPHOUS MATERIALS USING TIME-DOMAIN TERAHERTZ SPECTROSCOPY

BY

THOMAS E. REIN

B.S. ALFRED UNIVERSITY (2010)

SIGNATURE OF AUTHOR (Signature on File)

APPROVED BY (Signature on File)

ALEXIS CLARE, ADVISOR

(Signature on File)

S.K. SUNDARAM, ADVISORY COMMITTEE

(Signature on File)

MATTHEW HALL, ADVISORY COMMITTEE

(Signature on File)

CHAIR, ORAL THESIS DEFENSE

ACCEPTED BY (Signature on File)

DOREEN D. EDWARDS, DEAN
KAZUO INAMORI SCHOOL OF ENGINEERING

ACKNOWLEDGMENTS

I would first like to thank my advisor, Dr. Alexis Clare, for supporting me through my graduate studies, and for her constant willingness to help me succeed. Her contribution to this work has been invaluable, and I will always be grateful. I would also like to thank my committee members Dr. S.K. Sundaram, and Dr. Matthew Hall for their input as well to this work, and in general.

I would like to acknowledge Sean Breed for his contribution to writing this thesis and also technical support in the lab, Fiona Cormack and Karen Bond for lab support, Rob Koch for his contributions to Terahertz Spectroscopy, and Peter Metz for his support with X-Ray Analysis.

TABLE OF CONTENTS

LIST OF TABLES

Page

LIST OF FIGURES

Page

ABSTRACT

Terahertz Spectroscopy of glasses is a relatively new field due to recent developments in terahertz generation and detection. These high frequencies open a range of possibilities in terms of communication and electronic capabilities. In order to actually develop these technologies, an understanding of how materials react in this frequency range is necessary for both photonics and electronics. Oxide glasses are typically used for their optical properties and also are less subjected to electrical properties with respect to temperature and aging (i.e. higher reliability).

This study is based on alkaline earth modifiers in glass and its effect on Terahertz radiation. The alkaline earth modifiers used were barium oxide (BaO), strontium oxide (SrO), and calcium oxide (CaO). Sodium oxide modifier was also used to aid in forming the glass, and therefore the effects of sodium oxide addition are presented in this study as well.

In addition to the Terahertz effects, physical properties of each glass were characterized using Differential Scanning Calorimetry (DSC), Density (Archimedes method), Ultraviolet-Visible absorption (UV-Vis), and Infrared absorption (FTIR). The glasses were confirmed to be amorphous via X-Ray Diffraction. Differential Scanning Calorimetry is used to define the glass transition temperature (T_g), and density which gives insight to the glass structure and the effects in the Terahertz range. Ultraviolet-visible and infrared transmission were used to additionally characterize the glasses in terms of optics.

The manufacturer of the Terahertz Spectrometer had also given an alternative method of measurement where powders are mixed with transparent High-Density Polyethylene (HDPE). This process was explored with glass frit that was quenched by various methods to induce a change in structure. This was characterized through density; via Helium Pycnometery and also Differential Scanning Calorimetry.

Also characterized were the terahertz properties of ion-diffused commercial float glass, as well as glass thickness with respect to terahertz transmission. The paper also establishes practices for glass characterization of terahertz spectroscopy.

INTRODUCTION

The terahertz gap is a region of the electromagnetic spectrum that has been for many years unexplored due to the lack of a terahertz source.[1] This limited capabilities to analyze materials in this region and thus led to a split in the electromagnetic spectrum between far-infrared photonics and electronics. With the electronics industry moving steadily towards higher frequency to improve processor speeds, there is a need to understand the response of materials in the terahertz region to ensure safety and reliability of these devices. Glasses in particular are used as low-tolerance, high-performance dielectrics for capacitors for advanced electronics.[2-6] Also, the use of terahertz radiation is being considered for communications for a broader bandwidth to allow more information to be transferred in a given time.[7]

A. Instrument Background

The ability to construct a terahertz source has been a relatively new discovery, and previously, Far Infrared Spectroscopy (FIR) has been used to explore the terahertz range, but the signal to noise ratio (which is a ratio of power) for frequencies less than 3 THz is ~300.[8] Terahertz Time-Domain Spectroscopy (THz-TDS) has been reported to have a signal-to-noise ratio as high as $>10^8$ for frequencies less than 3 THz whereas the opposite is true for frequencies greater than 5 THz. The complex dielectric constant can be reliably calculated for Frequencies < 3 THz from the spectrum and sample thickness. While FIR has advantages over THz-TDS at frequencies above 5 THz, the focus of this work will be within the range of frequencies less than 3 THz.

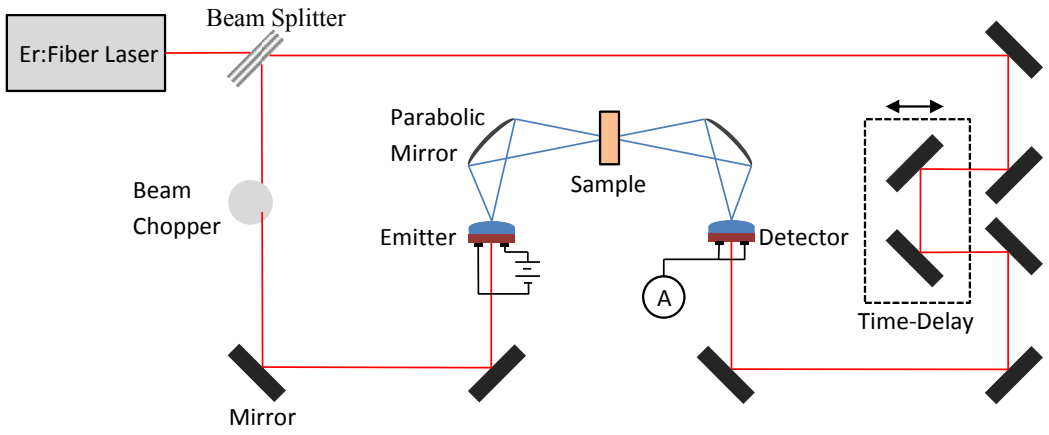

Figure 1. Schematic diagram of Terahertz Time Domain Spectroscopy.

Figure 1 shows the setup for the instrument where an erbium doped fiber femtosecond laser emits 780 nm laser pulses with less than 100 femtosecond pulse duration that splits into two beams. The first beam goes through a beam chopper then is reflected to the emitter. The emitter emits a pulse of THz radiation, which is then directed towards the sample. The signal is then reflected to the detector connected to a computer.

The Terahertz emitter is a photoconductor that employs a semiconducting GaAs/AlGaAs diode.[9] This material, when exposed to a short pulse (<90 fs for the instrument used in this study) laser under a DC biased voltage, generates a change in current which produces an electromagnetic wave in the Terahertz range. The radiation is then directed towards to the sample by means of parabolic mirrors then redirected towards the detector. The detector works similarly to the emitter with the exception that the electric field is generated by the incoming radiation, which alters the current. The high signal-to-noise ratio comes from the fact that the detector rejects incoherent radiation along with combining many averaging scans (e.g. 1000 scans).

The detected signal is expressed in terms of optical time delay, which can be Fourier Transformed from time domain into frequency domain. The spectrometer uses a Fast Fourier Transform with a range of apodization options (8 in the program that is available). The apodization functions are typically applied to remove or reduce measurement artifacts. For this study the Blackman-Harris 3 term apodization function is

used as a medium between apodization effects and is typically suitable for most applications (where Boxcar has no effect, and Norton-Beer Strong has the strongest effect). The apodization sacrifices some of the signal-to-noise ratio for resolution.

The difference in ratios of electric fields between the sample and the reference spectra reveals the refractive index (or refractive index difference) of the sample as well as the absorption coefficient.[10] This in turn calculates the dielectric constant of both its real part and imaginary part along with its phase. This study focuses on the absorption in terms of its coefficient, which accounts for sample thickness, and the complex dielectric constant.

B. Terahertz Radiation and Materials

It is well known that a frequency dependence exists for polarization within materials. This dependence is based upon the polarization effects from electronic (α_e), molecular (α_m), lattice (α_l), and space charge (α_{sc}) nature of materials.[11] It can be expected that at lower frequencies below the band gap that the dielectric constant will increase due to stronger effects from polarization. Since Terahertz radiation is associated with rotational movements of molecules, a combination of these polarization effects result in the dielectric constant of materials. General overviews for different types of materials are located below.

1. Organic Materials

Most research within the terahertz range has been with organic molecules where the long chains will absorb THz radiation in accordance with their structure.[12-15] In particular there has been much research within detecting and characterizing explosive materials for security applications.[13,16] This can be done because many explosive organic materials have a rotational vibration absorption peak, which is used as an identifier particularly at airports.

2. Crystalline Semiconductors and Insulators

Crystalline structures have a major effect on the optical and electrical properties of materials where long range order dominants these effects. Amorphous materials can have the same chemical composition but significantly different properties because of the lack of long range order. For example the most common dielectrics are crystalline ceramics with a tetrahedral perovskite structure because the center ion (such as titanium) located in the center of the structure spontaneously polarize giving rise to a high dielectric constant.[11,17-19] These materials are strongly subjected to tetrahedral perovskite structure which can change with respect to temperature to a cubic structure, and there has been some work on doping these materials to make them less sensitive to temperature.[20-22]

Crystalline materials such as silicon have been well studied and characterized in terahertz spectroscopy with a variety of dopants and forming processes to demonstrate the effects these changes make on the electric and optical properties.[23-29] For silicon itself lower terahertz frequencies are less transparent where at higher frequencies it acts more like quartz.[29] Adding dopants to change the electrical resistivity will also affect the absorption. Other semiconductors such as quartz, sapphire, gallium arsenide, and germanium have also been characterized. The effect of the crystalline structure for quartz increases the absorption compared to fused silica. Sapphire has higher absorption than quartz at values above 1 THz, but acts similarly in transmission in Terahertz frequencies <0.5 THz. Gallium arsenide has a couple weak absorption peaks at 0.4 and 0.7 THz indicating some structural effect. Germanium has been used to demonstrate the role of intrinsic carriers.

3. Metallics

Metals such as aluminum, silver, and gold have been studied in the Terahertz region and have been found to be reflective just as they are in the visible range.[30] This effect arises from overlaying valence and conduction band nature of most metals. It is generally accepted that reflection will occur with metals and therefore are suitable for Terahertz mirrors regardless of substrate.

4. Inorganic Glass

Glass inherently is known for its high transmission optical properties, low chemical reactivity, low electrical conductivity, and low thermal conductivity for typical soda lime silicate glass and since the start of terahertz spectroscopy, glasses have generated interest for the optical and electrical properties of glass in this region.[14,31-38] Common glasses such as soda lime silicates are used as containers for liquids that could potentially contain explosives. The terahertz radiation provides insight to the glass structure and is closely related to mechanical and optical properties of glass.[35] Thus far, glass is regarded as fairly transmissive in the terahertz region with fused silica having the highest transmission for oxide glasses. It is known that modifier additions change the amount of absorption with respect to frequency and thus the dielectric constant changes with it.[33] It is possible to extract the dielectric constant of the material from the thickness and polarizability of the glass as well.[35]

C. Glass Compositions and Structure

Much depends on the structure of the glass, which is influenced strongly by the composition and processing conditions.[39] The composition of the glass starts with the selection of a glass former, which provides a base for the glass to form. Silica being the most common former for oxide glasses ideally provides a network of silicon ions bonded by 4 bridging oxygen ions. The addition of a glass modifier forms non-bridging oxygens with the charge balanced by the modifier ion. Figure 2 outlines the theoretical number of bridging oxygens in Q_n notation where n is the number of bridging oxygens per tetrahedron for alkali oxide modifiers. While each alkali oxide ion must be neighboring one non-bridging oxygen, alkaline earth oxide ions must be neighboring two non-bridging oxygens. A modifier is usually added to lower melting temperature and achieve desirable properties due to the increase concentration of non-bridging oxygens and less connectivity of the glass structure. The addition of modifier also changes the polarizability of the glass, which directly relates to the dielectric constant.[40,41] The

increase in concentration of modifier atoms provides more polarizing locations in the glass.

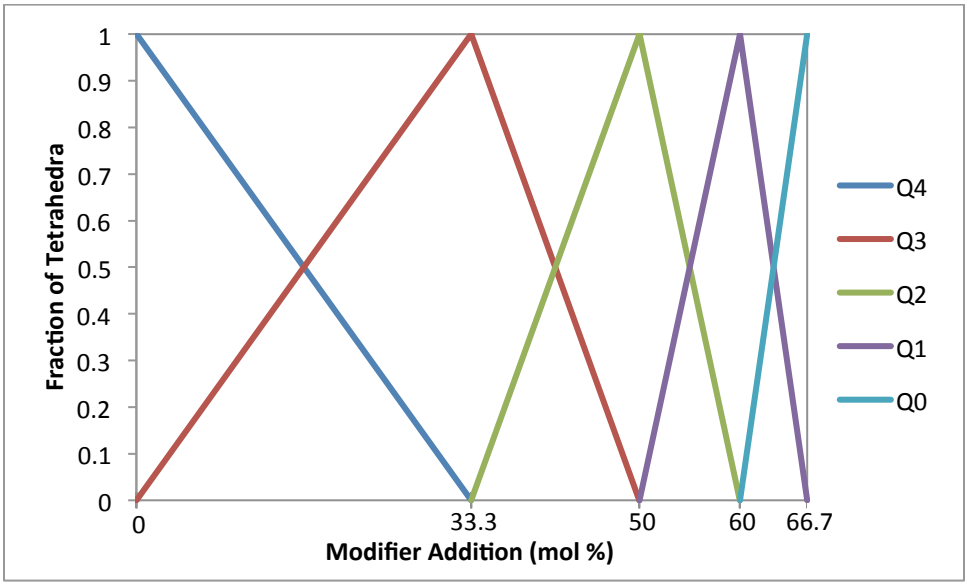

Figure 2. Effect of alkali oxide concentration on the relative theoretical concentrations of Q_n units in alkali silicate glasses.[39]

The type of modifier also influences the glass where high refraction (i.e. high polarizability) is a result of the charge of the modifier as well as its size.[41] Also the average electron density is increased by most modifiers. Modifiers with larger ion electron clouds are able to shift (polarize) more than their smaller related group members however; some glass constituent such as fluorine and boron lower the electron density and cause a shift to lower refractive index.[39] The electron density dictates the response from the four types of polarization, which all affect the material response in Terahertz spectroscopy as each type of transition has enough response time at relatively low terahertz frequency (compared to visible light).

Glass structures are highly dependent on their processing conditions as well.[39] The cooling process is what actually forms a glass where a melt "freezes" the structure before it can crystalize. Due to the poor thermal conductivity of glass during cooling, the outside of a glass sample cools faster than the inside.[42] This forms a stress gradient which affects the polarizing nature of glass.[43,44] This can cause localized shifts in refraction or

polarization in a preferred orientation, which can be mistaken for absorption in spectroscopy. To relieve the glass from this stress, it is heated to a point just around the glass transition temperature to allow the ions in stressed condition to shift around a more energy conservative environment (i.e. little to no stress). Some glasses build up too much stress and form a facture due to the stress gradient, and other glasses have stress that exists in the glass, but require a defect (typically at the surface) in order to commence a fracture. Since this strain is a factor in polarization it has to be taken into consideration during testing.

D. Dielectric Properties and Polarizability of Glass

As described in the previous section, dielectric constant and polarizability are heavily dependent on composition and processing conditions.[45] The dielectric constant and polarization also are a function of beam energy (i.e. wavelength/frequency) and ambient conditions. The radiation type influences what energy can invoke what reaction from a material. For the case of glass most studies are in ultraviolet-visible spectrum because of its high transmission. Minimal radiation in the visible range is absorbed unless the glass contains a dopant that absorbs by electronic transition(s).[46] These transition absorption peaks typically appear as color in the glass, but otherwise glass usually appears clear. In the ultraviolet range, where energy is greater, significant absorption occurs from the greater energy invoking electronic transitions.

The infrared spectrum for silicate glasses usually contains some information on the bonding nature of the glass caused by absorbed energies from vibrational states of bonds.[47,48] Infrared radiation is commonly known for characterizing Si-O bonds and -OH groups (from ambient humidity). The multiphonon edge or IR cutoff is another feature in infrared spectroscopy for glasses and represents the limits of the spectrum that can be used to transmit radiation. These edges are caused by fundamental vibrations and overtones between ions that make up the glass structure.[39]

Glasses generally have high transmission for microwave radiation.[49] This gives glasses an advantage for high frequency electronics due to the lack of absorption bands and a relatively consistent dielectric constant over a range of microwave frequencies. It

also makes glasses practical for applications such as containers in microwave ovens in which transparency is required to heat food evenly. There still exists a slight interaction but the response to the radiation is minimal. A similar effect occurs also for radio frequencies.

To expand electronics and optical windows to include terahertz frequencies makes it necessary to know how materials will respond to the frequencies. Dielectric materials can be tailored to achieve certain properties by additions to a base material. Glass additions are usually in the form of modifiers and intermediates to a glass former whereas for common dielectric materials dopants are added to a based material such as barium titanate.

In terms of applications the non-crystalline nature of glass provides some major advantages over typical dielectrics for capacitors. The first is that glass dielectrics have extremely low dependency on temperature of capacitance (~5 ppm/°C – For comparison a C0G capacitor, which has the tightest restrictions for temperature, is < 30 ppm/°C).[40,50,51] Ceramic dielectrics depend on their crystal structure for dielectric behavior by creating regions of free space for electron clouds to shift to, so a change in crystal structure easily changes the behavior.[11] Barium titanate is a ceramic that has the highest dielectric constant and usually is doped to adjust for lower temperature dependency. Barium titanate is a tetragonal crystal at room temperature that polarizes due to titanium ions located at the center of a perovskite structure. This crystal structure changes at about 125 °C into a cubic structure that greatly reduces the polarizing nature of titanium ions by equalizing the distance between bonded oxygen ions. Glass can be used at higher temperatures (~200 °C) because it has no long-range structure which eliminates the crystal structure dependence and maintains a more constant capacitance value.

Glass also provides three other major advantages over ceramics in terms of dielectrics for capacitance: No aging rate, low chemical reactivity from the environment, low failure rates/high reliability.[50] Aging effects arising from changes by means of relaxation or realignment of electrical dipoles from external electric fields are common with some ceramic capacitors, and can damage equipment if the change becomes too great. Common glass, such as soda-lime-silicate, is also known to be chemically inert compared to most materials.[52,53] A material is never totally inert, but erosion from

ambient environment is extremely low for common glasses (glasses can also be designed for high reactivity). Finally, the non-crystalline, homogeneous nature of glass maintains a consistent and predictable dielectric failure rate when subjected to an electric field. Glass capacitors are known to be highly reliable, but do have a higher cost associated with them over their ceramic counterparts.

Ion diffused layers of potassium and silver in soda lime silicate glass are of interest due to the change in stresses at the surface of the glass as well as electrical and polarizability properties.[54-57] It is evident for silver that in the visible range for these glasses there is absorption, but this study will focus on the effects in the terahertz region. Terahertz radiation is considered low-frequency in terms of photonics and high frequency in terms of electronics. The remainder of this thesis will regard terahertz as high frequency to remain consistent with the scope of this work.

E. Design of Experiment

The purpose of this experiment was to characterize the polarization/dielectric effects of individual glass modifier ions in alkali/alkaline earth silicate glasses with terahertz radiation. Specifically there are four different focuses: (i) ion size and concentration of alkaline earth modifiers using the elements calcium, strontium, and barium; (ii) the influence of sodium modifier in these glasses; (iii) alternative methods of testing for use of thermally induced stress in glass; (iv) comparison with commercially available float glass with and without ion exchanged surfaces.

Since the dielectric constant of materials in the terahertz region directly relates to polarizability, experimentation can be based on electron density of the glass via ion size, ion oxidation state, and concentration, which affects the atomic structure. The ion oxidation state within investigation for this study is the 2+ oxidation state of the alkaline earth oxides. Varying concentrations of each ion are used in each glass in increments of 5 mole % and replacing silicon oxide glass former (since fused silica is known to have high transmission of THz light) as outlined in Table I. For realistic processing, sodium oxide was added to reduce melting temperature, but is kept at 20 mole % for each glass.

Table I. Design of Experiment to Compare Ion Size and Concentration of Alkaline Earth Oxides

Ion Size (Type)	**Concentration of alkaline earth oxide**					
		5 % mol.	*10% mol.*	*15% mol.*	*20% mol.*	*25% mol.*
	*Ca (100 pm)**	NaCa-5	NaCa-10	NaCa-15	NaCa-20	NaCa-25
	*Sr (118 pm)**	NaSr-5	NaSr-10	NaSr-15	NaSr-20	NaSr-25
	*Ba (135 pm)**	NaBa-5	NaBa-10	NaBa-15	NaBa-20	NaBa-25

* Effective Ionic Radii[58]

Sodium oxide still influences the dielectric constant and polarization, so to measure that effect, three compositions that vary sodium oxide were used with a consistent amount of 20 mole % of barium oxide for each glass. The glass compositions are outlined in Table II. At low concentrations of sodium oxide, the melting temperature is extremely high for the furnace used in this study so the range of glasses was not expanded out to include sodium oxide concentrations of 5 and 10 mole %.

Table II. Design of Experiment for Varying Sodium Oxide Levels

Concentration of alkali oxide			
	15 % mol.	*20% mol.*	*25% mol.*
*Na (102 pm)**	BaNa-15	BaNa-20	BaNa-25

* Effective Ionic Radii[58]

Strain within glass can cause a polarization of light passing through the medium, which commonly occurs due the glass melting process. In order to relieve the glass of these strains, heat treatment (annealing) of the sample occurs near the glass transition point. Depending on the glass, some strain still develops -even if it is slight- near to surface of the glass. Glasses that are fast quenched (i.e. unannealed) are known to build up excessive stress between the surface and the bulk of the glass. This stress causes the glass to be ineligible for cold-working (i.e. cutting, grinding, and polishing) as the glass will fracture during working. Since such strained glasses are difficult to fabricate without cracks and is difficult to measure a sample to model the effects of strain on the glass,

however; a strained glass can be purposely crushed into a powder, and the Terahertz Spectrometer manufacturer has developed a procedure to use powders in the spectrometer. By crushing the powder it relieves the bulk glass stress, but local stress still exist. Scattering of the powders, for this experiment, is reduced by using a reference sample of the highly THz transmissive material high density polyethylene (HDPE), which is used as the binder of the glass frit. This procedure was used with glass frit which has purposely thermally induced stress within the glass structure. This is achieved by quenching glass at different rates. Each quenching method used for this experiment is noted in Table III for a single composition.

The procedure outlined by the manufacturer uses a high THz transmission material (i.e. high density polyethylene) mixed with a powdered form of the material being studied (glass frit for this experiment). The mix is then pressed into a pellet that is about 1.5 mm thick, then used as a sample in the spectrometer. The polyethylene also serves as a binding medium so the sample does not break easily during handling.

Table III. Design of Experiment for Glass Processing Quench Method

Quench Method			
	Annealed	*Air Quenched*	*Water Quenched*
NaBa-15s	NaBa-T-AN	NaBa-T-AQ	NaBa-T-WQ

Additionally the effects of ion exchanged elements provide surface and subsurface changes of the properties. Such an example is chemical strengthening of glasses by replacing sodium ions at the surface of the glass with larger potassium ions to form a compressive surface. Silver is also another ion that readily diffuses into the surface of glasses and can cause discoloration in the visible range by the formation of nanoparticles in the glass. These glasses are subjected to Terahertz radiation using diffused silver and potassium at the two surfaces of commercially available float glass. These glasses are outlined in Table IV with the heat treatment temperature for 1 hour.

Table IV. Design of Experiment for Silver/Potassium Ion-Exchanged Commercial Glass

Heat Treatment			
	Untreated	*350 ℃*	*550 ℃*
SLS	AgK-UT	AgK-350	AgK-550

X-Ray diffraction is commonly used to confirm general amorphous structure of glass. Density of the glass is measured using Archimedes method to provide some insight into the structure of the glasses. Differential Scanning Calorimetry is also employed for glass transition temperature measurements, which also aids in providing insight into the glass structure. Ultraviolet-Visible Spectroscopy and Infrared Spectroscopy were used for comparison to Terahertz Spectroscopy.

EXPERIMENTAL PROCEDURE

A. Glass Compositions

The design of the experiment primarily focuses on modifier ion size as well as total concentration. To form the glasses at the desired temperature and conditions, a glass network modifier was utilized to form an amorphous structure, which in this experiment was sodium oxide in combination with the alkaline earth oxide. Since sodium oxide was used for this experiment it was important to note the effects of sodium concentration with alkaline earth modifiers as well. So a separate series with a constant concentration of barium oxide at 20 mole % was used to describe the effect of sodium oxide in the glass. Also explored, was the effect of stress from the cooling process using a method described by the Terahertz Spectrometer manufacturer where glass frit was milled and mixed with high density polyethylene (HDPE) powder.

Table V, Table VI, and Table VII outline the glass compositions used in the compositional effects study where the varying modifiers were barium, strontium, and calcium respectively. Table VIII outlines the compositions for the series where sodium was the varying modifier. Some compositions in the variable sodium series described in Table VIII were omitted due to forming issues that require high temperatures, which related to the low modifier content.

Table V. Glass Compositions for NaBa Series Glasses (in mole percentage)

Glass	SiO_2	Na_2O	BaO
NaBa-5	75	20	5
NaBa-10	70	20	10
NaBa-15	65	20	15
NaBa-20	60	20	20
NaBa-25	55	20	25

Table VI. Glass Compositions for NaSr Series Glasses (in mole percentage)

Glass	SiO_2	Na_2O	SrO
NaSr-5	75	20	5
NaSr-10	70	20	10
NaSr-15	65	20	15
NaSr-20	60	20	20
NaSr-25	55	20	25

Table VII. Glass Compositions for NaCa Series Glasses (in mole percentage)

Glass	SiO_2	Na_2O	CaO
NaCa-5	75	20	5
NaCa-10	70	20	10
NaCa-15	65	20	15
NaCa-20	60	20	20
NaCa-25	55	20	25

Table VIII. Glass Compositions for BaNa Series Glasses (in mole percentage)

Glass	SiO_2	Na_2O	BaO
BaNa-15	65	15	20
BaNa-20	60	20	20
BaNa-25	55	25	20

The glass composition series outlined in Table IX shows the composition for each glass as well as the quench method used. The differences in these processes were characterized by means of helium pycnometery for density and glass transition temperature through differential scanning calorimetry.

Table IX. Glass Compositions for NaBa-T Series Glasses (in mole percentage)

Glass	SiO_2	Na_2O	BaO	Quench Method
NaBa-T-WQ	65	20	15	Water
NaBa-T-AQ	65	20	15	Air
NaBa-T-AN	65	20	15	Annealed

B. Sample Preparation

All glasses were batched using an A-160 Scale (Denver Instrument GmbH, Göttingen, Germany), and formed in a 10% Rh-Pt crucible using a Carbolite HTF 17/5 furnace (Carbolite, Watertown, WI) at 1500 °C for 2 hours. For compositions described in Table V, Table VI, Table VII, and Table VIII the glasses were poured onto a steel plate at room temperature then annealed on a preheated zirconium oxide refractory in a Thermolyne 48000 furnace (refractory preheated to annealing temperature). Glasses were annealed at 20 °C above the T_g for 2 hours then cooled at a rate of 1 °C/min for the first 300 °C, then allowed to cool in the furnace to room temperature.

THz-TDS is sensitive to the sample thickness. For the varying composition series it was recommended that glass samples should be about 1 mm thick, but samples up to about 4 mm are visible. These samples can also be used for UV-Visible Spectroscopy, Infrared Spectroscopy, and Density measurements. Glasses were cut then polished by hand gradually to 1 μm diamond paste.

Glasses in Table IX were formed in the same crucible and furnace with the same parameters. The annealed and air quenched samples were poured onto steel at room temperature. The annealed sample used the same annealer and cycle as the previous glasses. The water quenched sample was left in the crucible and placed into water without the water touching the glass itself. These glasses were crushed up into a powder, and sieved to less than 75 μm. The powder was mixed with high density polyethylene (HDPE) powder at 20 % wt. into pellets of 90 mg of glass frit and 360 mg of HDPE powder. A sample of 360 mg of HDPE only was used for a reference. These powders

were pressed into pellets of 19 mm diameter at 2 metric tons, and then weighed after for any material loss due to adhesion weighing containers.

For ion-exchanged glasses a mixture of 1:1 mole % silver nitrate to potassium nitrate was mixed with EPK Kaolin and coated onto commercially available float glass which was processed by skimming the melt on a molten tin bath (Guardian Glass, Geneva, NY). Glasses were heat treated in a Thermolyne 48000 furnace at temperatures of 350 ℃ and 550 ℃.

C. X-Ray Diffraction

To confirm amorphous structure of the glasses created in the lab, X-Ray Diffraction was used to verify that no crystalline phases were present. To do this, a D2 Phaser X-Ray Diffractometer (Bruker AXS, Karlsruhe, Germany) was employed. Samples were milled into powder form prior to X-Ray analysis. A spectrum from 20.000 to 80.017 °2θ with a step size of 0.051 °2θ and 1 s/step was measured. The sample was rotated at 30 rpm, and X-Rays were generated using Cu tube at 20 kV potential and 10 mA current. Analysis of the data used Cu-$K_{\alpha 1}$ rays with X'Pert HighScore Plus software (ver. 2.2a(2.2.1), PANalytical B.V., Almelo, The Netherlands). A schematic overview of the instrument is shown in Figure 3, where a Cu X-Ray source and detector are moved to change the angle at which the x-rays diffract.

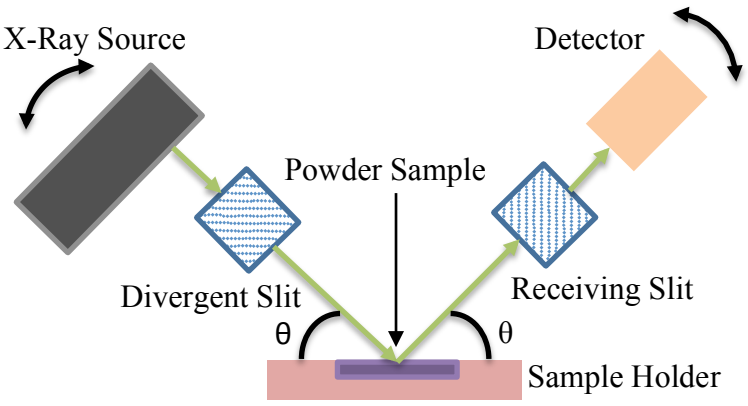

Figure 3. Schematic diagram of X-Ray powder diffraction.

D. Density

The free volume of the samples influences the space for individual ions to polarize, thus to characterize this free space, density measurements need to be taken. Due to slight differences in geometry the Archimedes Principle method provides an accurate way to model the free volume. Figure 4 shows the schematic diagram for the method where three measurements are taken: dry mass (m_{dry}), suspended mass ($m_{suspended}$), and temperature of fluid. Five samples were used for each glass compositions to ensure accuracy. The density of the fluid (ρ_{fluid}) is dependent on the temperature, and therefore temperature is measured. The fluid used in this experiment is kerosene where the density is known for given temperatures.

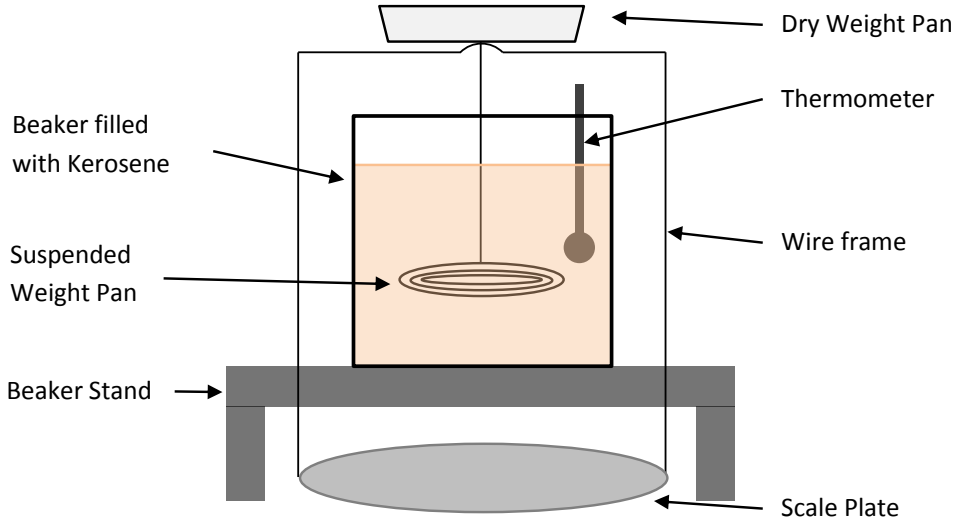

Figure 4. Schematic diagram of Archimedes principle density measurement.

Equation (1) describes the method for calculating the density of the sample. This equation is for glasses that are non-porous and bubble-free.

$$\rho_{sample} = \frac{m_{dry}}{m_{dry} - m_{suspended}} \cdot \rho_{fluid}(T) \quad (1)$$

For the glass frit described in Table IX, a AccuPyc II 1340 helium pycnometery (Micromeritics, Norcross, GA) was used to obtain the density since the frit is in powder form and cannot be measured with Archimedes method using the set up described in Figure 4. Five measurements for each sample were taken to establish average density with error. Errors can arise due to pressure changes within the technique, along with ambient conditions.

E. Differential Scanning Calorimetry

To correlate compositional and thermal history for the glasses DSC was employed to quantify a glass transition temperature (T_g). Glass preparation included milling into powder form to allow thermal energy to distribute more evenly in the sample and create more surface area.

A 2910 DSC (TA Instruments, New Castle, DE) was used to analyze the samples. Samples were heated to 550-600 °C at a heating rate of 10 °C/min in Aluminum pans. Nitrogen gas was used at a flow rate of 15 mL/min. Data were recorded as the temperature increased and completed when the maximum temperature was reached. Data analysis consisted of determining an onset point of that glass transition region in a plot of heat flow versus temperature.

F. Ultraviolet-Visible Spectroscopy

Ultraviolet-visible radiation stimulates electron transitions commonly utilized to determine the energy to jump valence electrons to an excited state, which is known to relate to the band gap of common glasses. For this study a Lambda 950 UV/Vis spectrometer (PerkinElmer, Akron, OH) was used with a scan range of 800 nm to 300 nm at 1 nm steps. The scan rate was 266.75 nm/min with a slit width of 2 nm. Scans were

taken at room temperature and conditions. Three scans were averaged together to obtain the results presented in the results and discussion section.

Figure 5 outlines the basics of the UV-visible spectrometer used. Two light sources emit ultraviolet, visible, and near-infrared radiation, which is passed through a diffraction grating and a narrow slit allows only a small band of light through, where the band is split into two beams. One beam is transmitted through the sample and the other passes through an empty sample slot. The two beams then redirect to the detector, which connects to a computer and measures transmission.

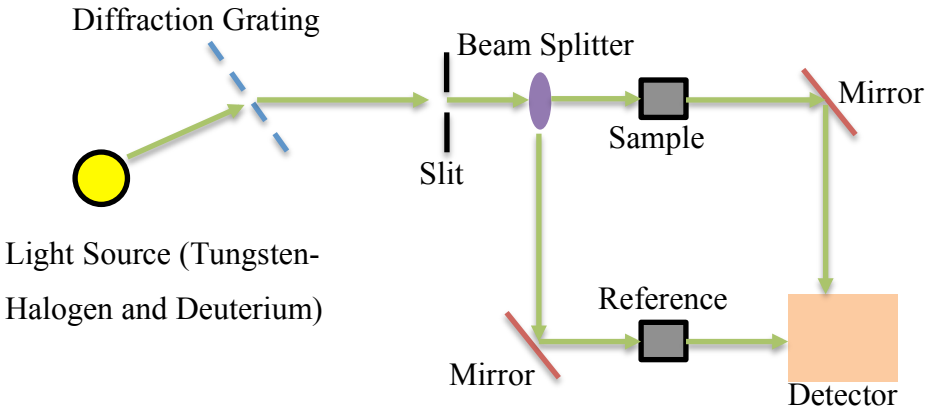

Figure 5. Schematic diagram of ultraviolet-visible spectrometer.

G. Infrared Spectroscopy

Infrared Radiation is associated with transitions due to molecular vibrations. A Nicolet 6700 FTIR Spectrometer (Thermo Electron Corporation, Waltham MA) was used with a scan range of 7400 to 350 cm^{-1} and a resolution of 4 cm^{-1}. Ninety scans were taken in transmission mode using H_2O and CO_2 correction as well as Mertz Phase correction. A Happ-Genzel apodization was applied to the spectrum. The overall spectrometer function is outlined in Figure 6 where an infrared light source was used in conjunction with an interferometer to generate a time-domain signal that is Fourier transformed into the frequency domain.

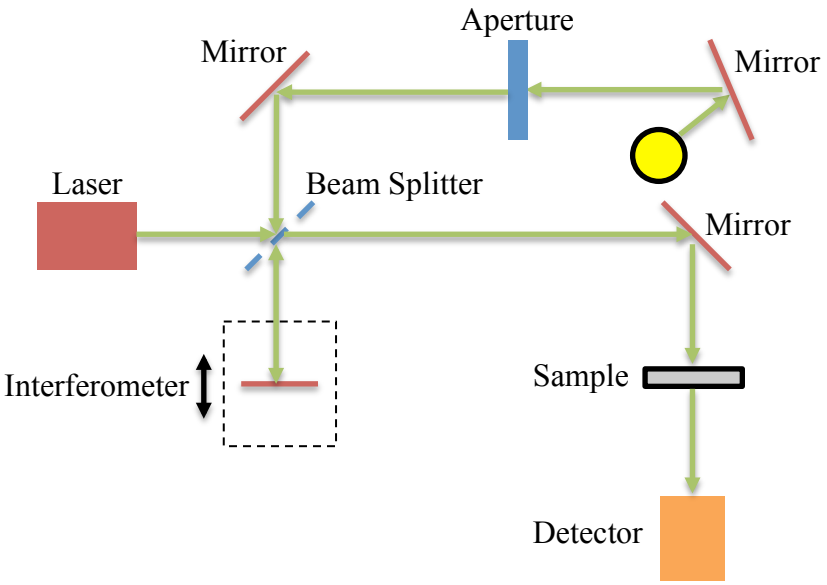

Figure 6. Schematic Diagram of Fourier-Transform Infrared Spectrometer.

H. Time-Domain Terhartz Spectropscopy

A TeraView TPS Spectra 3000 Spectrometer was used to measure Terahertz adsorption as well as dielectric constant for each of the samples. One thousand scans were used in transmission mode with a resolution of 1.200 cm^{-1} wavenumber and a scan frequency of 30 Hz. A Blackman-Harris 3 term apodization was applied to the spectrum. Dry high purity nitrogen gas was used to reduce water vapor in the sample chamber at a flow rate of 15 L/min. The details of the instrument are highlighted in the Introduction as well as Figure 1.

RESULTS AND DISCUSSION

A. Results and Discussion for X-Ray Diffraction

Figure 7 shows the X-Ray Diffraction pattern for the sodium barium silicate where barium concentration is the variable. The patterns are offset to show that the entire series is amorphous, as confirmed by the presence of an amorphous hump, or lack of any sharp peaks that would be present for a crystallite. Figure 8 shows the same pattern for the sodium strontium silicate series with variable strontium showing the same features. The same is also present for the sodium calcium silicate series in Figure 9.

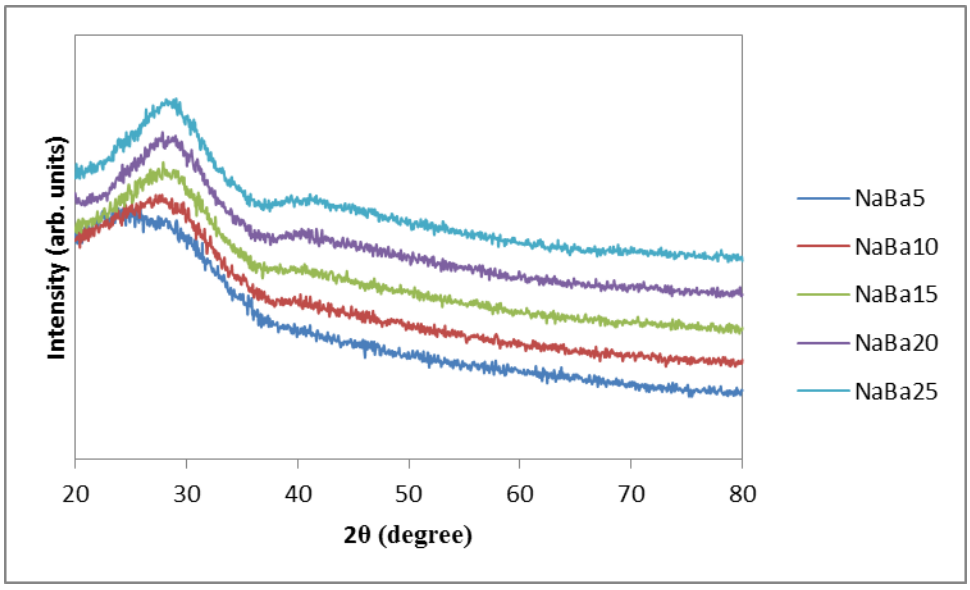

Figure 7. X-Ray Diffraction pattern for sodium barium silicate series with variable concentration of barium. Data series are offset for clarity.

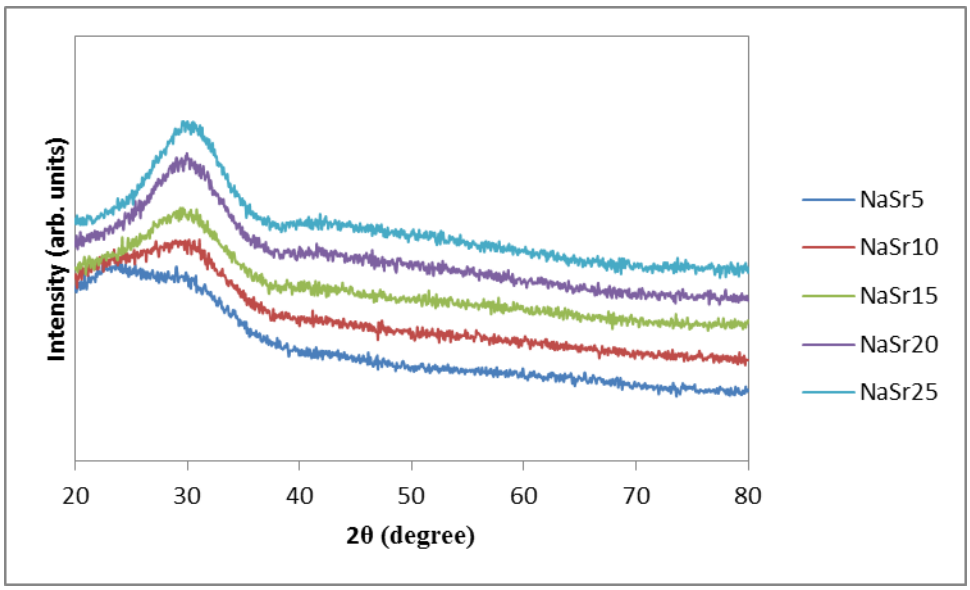

Figure 8. X-Ray Diffraction pattern for sodium strontium silicate series with variable concentration of strontium. Data series are offset for clarity.

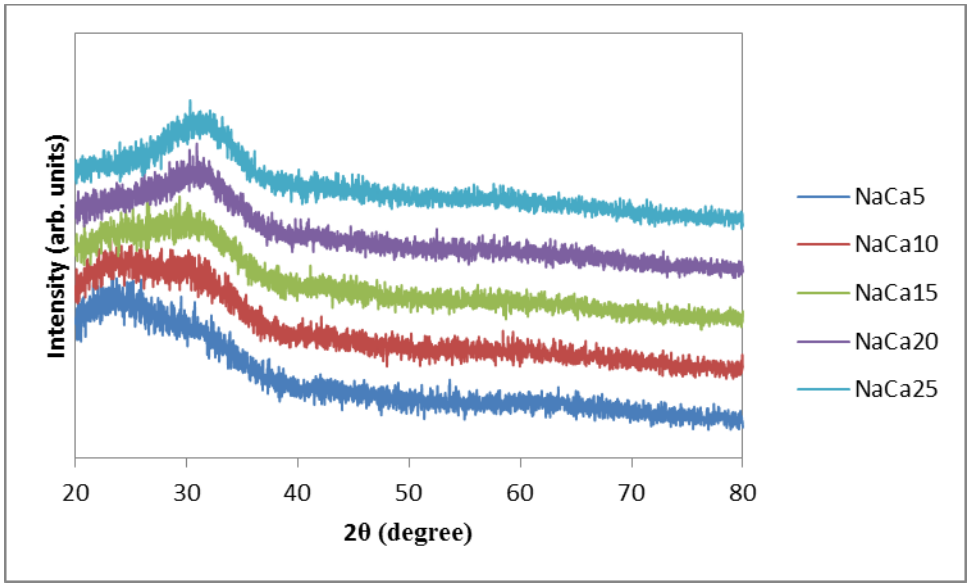

Figure 9. X-Ray Diffraction pattern for sodium calcium silicate series with variable concentration of calcium. Data series are offset for clarity.

Figure 10 shows an interesting feature with increasing sodium oxide content. As sodium oxide concentration increases, the amorphous hump peak shifts to a higher 2θ. The peaks are at 26.528 °, 27.293 °, and 28.517 ° 2θ for BaNa-15, BaNa-20, and BaNa-

25 respectively. This peak shift is associated with the medium range order of the glass structure and is a topic of debate in the scientific community.[59-63]

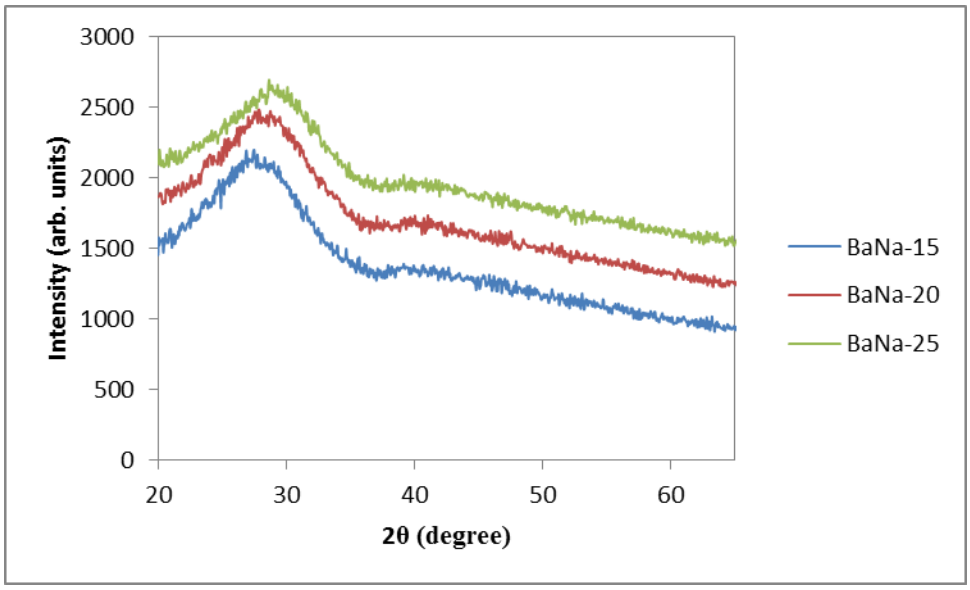

Figure 10. X-Ray Diffraction pattern for sodium barium silicate series with variable concentration of sodium. Data series are offset for clarity.

B. Results and Discussion for Density

Figure 11 shows the plot for density with respect to the increase in modifier content. In series 1 (NaBa), series 2 (NaSr), and series 3 (NaCa) the density increases with respect to the increase in the variable modifier. The second observation is the density increases with respect to the change in series (i.e. different size modifier). Series 4 (BaNa) shows a slight but not a definitive increase in density as sodium modifier content increases.

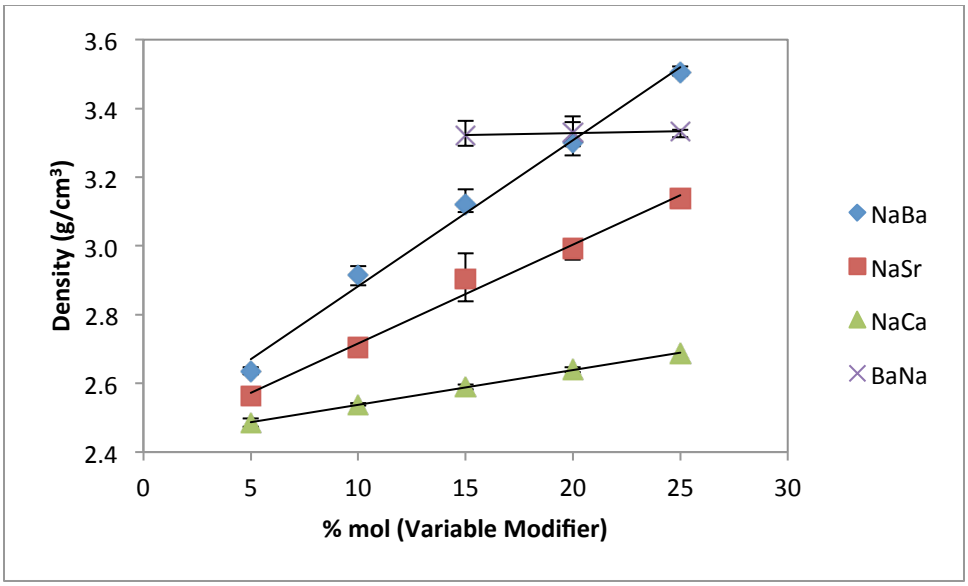

Figure 11. Density plot comparing all series of glasses.

The increasing density for Series 1, 2, and 3 (NaBa, NaSr, and NaCa respectively) can be attributed to the occupation by divalent alkaline earth ions in interstitial space within the glass network. With the increase in concentration of these ions, the density of the glass also increases. The type of alkaline earth ion also causes an increase in density as well. As the atomic number of the alkaline earth series increases the density also increases. This implies that the mass difference is greater than the volume change resulting in a higher density. Series 4 (BaNa) however does not share the same explanation because sodium ions decrease the molar volume of the network as well as occupy the interstitial space. It is known that the increase in concentration of sodium modifier does increase the density, but the increase is slight.[39]

Variations in the data can come from the thermal history of the glass as well. The cooling nature of the glass can fluctuate the volume based on the cooling rate of the bulk glass. Microbubbles, and bubbles can greatly change the data so samples were selected that were free from these defects. Slight variations in size of the glass, placement in the annealer, furnace parameters, and ambient conditions can cause a difference in data though care was taken to reduce these processing effects through means of consistent procedure, and tight tolerances in weighing raw materials.

C. Results and Discussion for Differential Scanning Calorimetry

Figure 12 show the Differential Scanning Calorimetry of the sodium barium silicate series, where the glass transition temperature is featured at the beginning of the endothermic peak. An onset point at this curve was used to characterize the glass transition temperature for each of the series in Figure 13.

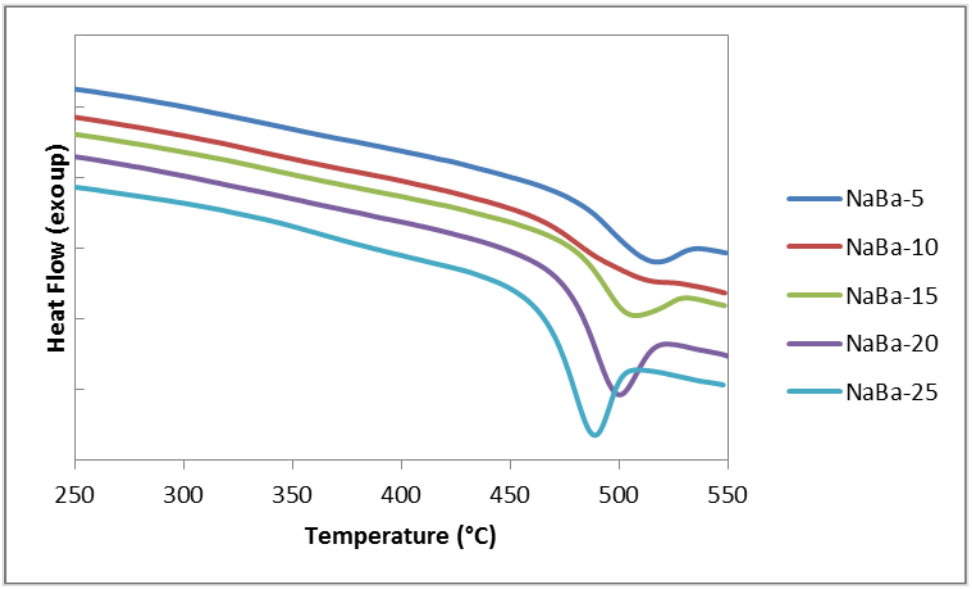

Figure 12. Differential Scanning Calorimetry scan for sodium barium silicate series with barium as the variable modifier. Data series are offset for clarity.

From Figure 13 it is evident that as the average modifier ion size of each series increases, the glass transition temperature decreases. The rise and fall in the sodium barium silicate, sodium strontium silicate, and sodium calcium silicate series is consistent with the liquidus temperatures for these compositions calculated by Dluegel's model.[64] This effect arises from the mix of alkali modifiers (i.e. Na_2O) and alkaline earth modifiers (i.e. BaO, SrO, and CaO). The apparent linear decrease in the barium sodium silicate series is directly attributed to the addition of Sodium modifier forming non-bridging oxygens and thus inferring that less energy is needed to form a melt.[39]

Glass Transition though is sensitive to thermal history as presented in Table X, where higher quenching rate increases the glass transition temperature. Table X shows the glass transition temperature for different quenching methods of the same sodium barium composition described in Table IX. Also slight variations in the composition due to volatilization can alter the transition temperature.

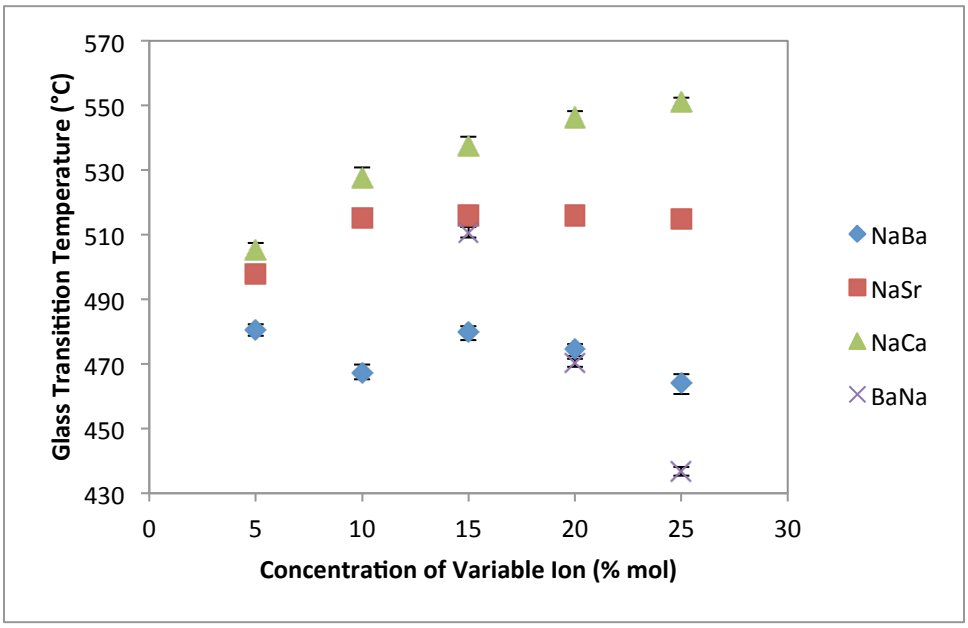

Figure 13. Glass transition temperature as a function of variable ion concentration (Ba, Sr, Ca, and Na) as determined by Differential Scanning Calorimetry.

Table X. Glass Transition Temperature for various Quench Methods

Quench Method	**Average T_g**	**Maximum T_g**	**Minimum T_g**
Annealed	461 °C	462 °C	460 °C
Air Quenched	464 °C	465 °C	462 °C
Water Quenched	468 °C	470 °C	467 °C

D. Results and Discussion for Ultraviolet-Visible Spectropscopy

Figure 14, Figure 15, Figure 16 and Figure 17 show the Ultraviolet-Visible spectrum for the sodium barium silicate, sodium strontium silicate, sodium calcium silicate and barium sodium silicate series respectively. The absorption spectra were normalized to 1 mm thickness to account for differences in sample thickness. The spectra remain generally featureless with the exception of the UV-edge, which ranges from about 300-350 nm for each series.

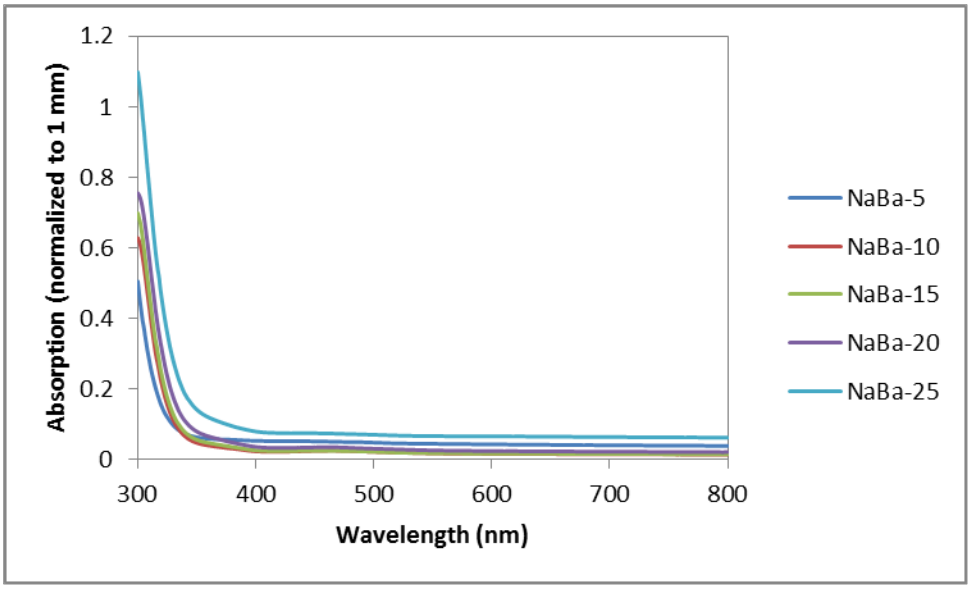

Figure 14. Ultra-Violet spectroscopy spectrum for sodium barium silicate series with barium as the variable modifier.

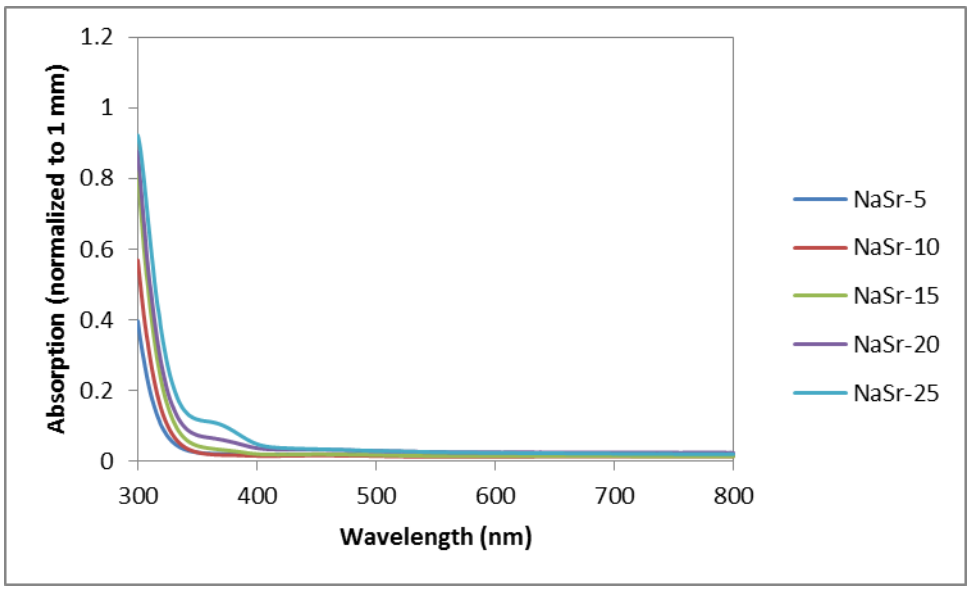

Figure 15. Ultra-Violet spectroscopy spectrum for sodium strontium silicate series with strontium as the variable modifier.

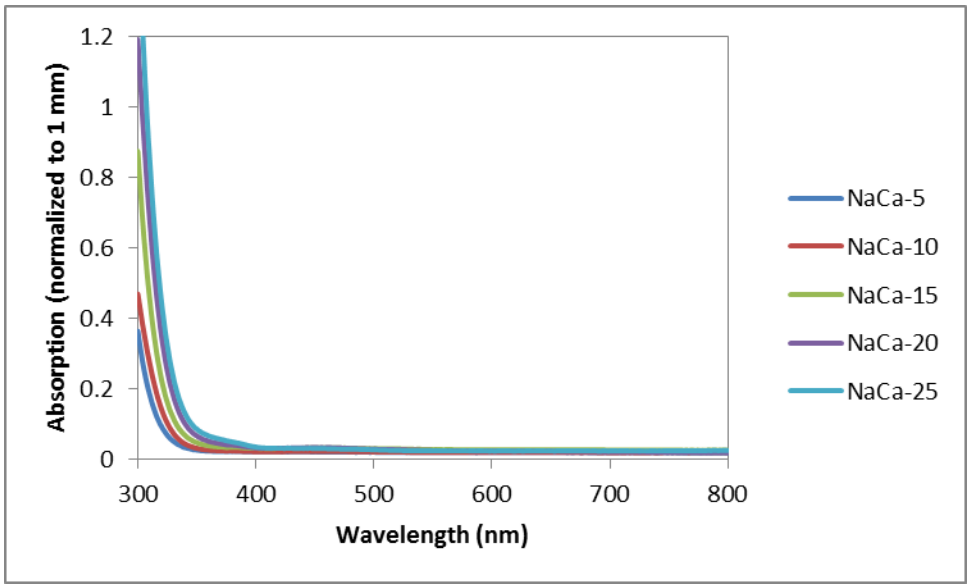

Figure 16. Ultra-Violet spectroscopy spectrum for sodium calcium silicate series with calcium as the variable modifier.

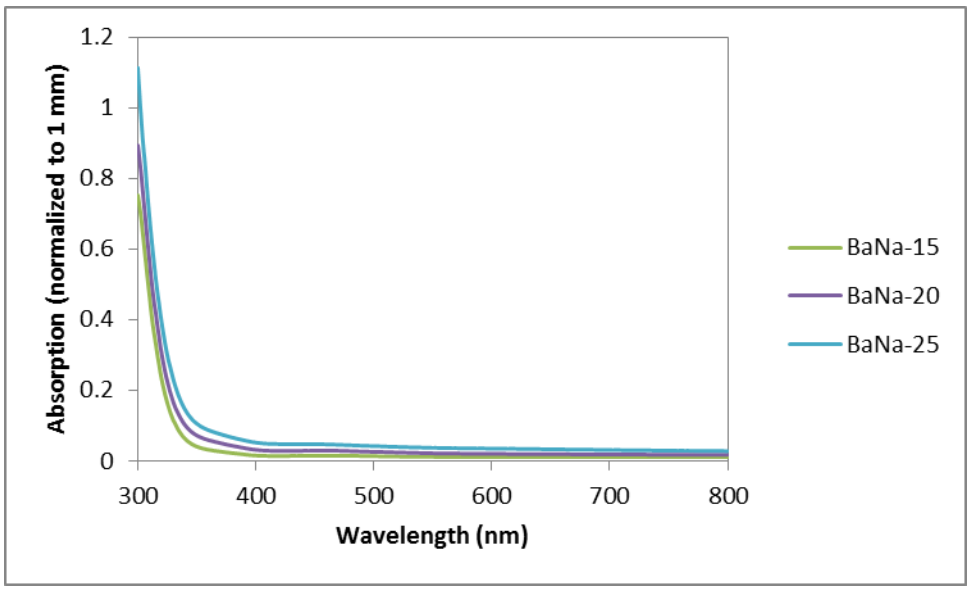

Figure 17. Ultra-Violet spectroscopy spectrum for barium sodium silicate series with sodium as the variable modifier.

It is noticeable that there is a shift in the UV-edge with respect to variable ion concentration. As modifier content increases for each composition, the UV-edge shifts to a higher wavelength (i.e. lower energy). To quantify this effect Table XI shows the wavelength value where the absorption is 0.2 for each millimeter. In the table there are two other trends to note: The UV-edge shifts to higher wavelength (lower energy) with respect to an increase in ion size, and the increase UV-edge wavelength with the increase in modifier content. The other feature of interest is the absorption peak at ~380 nm for some spectrums. This arises from the ferric $^4D_5$ transition from iron impurities that are sourced from the steel plate that the glasses were poured on as well as iron is a common contaminant in batch chemicals.[65]

Table XI. Wavelength at 0.2 Absorption for comparison of UV edge for each series

% mol variable ion	NaBa	NaSr	NaCa	BaNa
5	315 nm	310 nm	308 nm	-
10	321 nm	315 nm	314 nm	-
15	322 nm	321 nm	321 nm	322 nm
20	327 nm	324 nm	328 nm	327 nm
25	337 nm	330 nm	332 nm	332 nm

The UV-edge is known to be associated with the valence electron of an anion, in this case oxygen, to an excited state.[39] This effect becomes more predominate when there are more non-bridging oxygens (NBOs) present. Network modifiers are used to form NBOs and ultimately reduce the melting temperature of a silicate glass. Special topics of the mixed alkali effect are important to note, but do not apply in this study. From Table XI this effect is evident, and the shift in the UV-edge is directly proportional to the electronic band gap of the glasses. The wavelengths in this test focus on photon-electronic transitions, and the important point of this study in relation to terahertz spectroscopy is the characterization of electronic polarization contributions.

E. Results and Discussion for Infrared Spectropscopy

It is important to note that glasses are not fully chemically inert, and quite often are subjected to attack from water.[66,67] Reactive cations in the glass will form hydroxyls, which have a vibrational frequency in the infrared region of the electromagnetic spectrum. Therefore water interaction with glass can be characterized via Fourier Transform Infrared Spectroscopy (FTIR). Additionally glass bonds also have absorption activity in the infrared region.

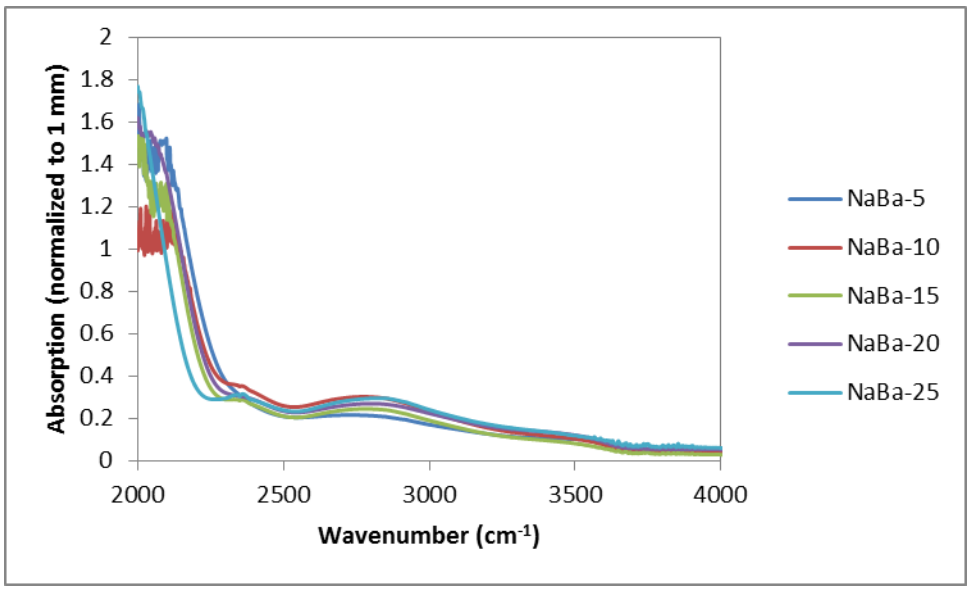

Figure 18. Fourier Transform Infrared spectroscopy spectrum for sodium barium silicate series with barium as the variable modifier.

It is unrealistic to form a glass completely free of water interaction, and thus evidence of water interaction during melting from ambient humidity is evident in Figure 18. Three peaks at about 3390, 3780, and 2325 cm^{-1} are present in each of the samples, which correlate directly to hydroxyl absorption. The same evidence is also present in Figure 19, Figure 20, and Figure 21. The hydroxyl absorption comes from ambient humidity and water used for processing during melting which trapped hydroxyl groups in the bulk of the glass and could affect results within the terahertz region.

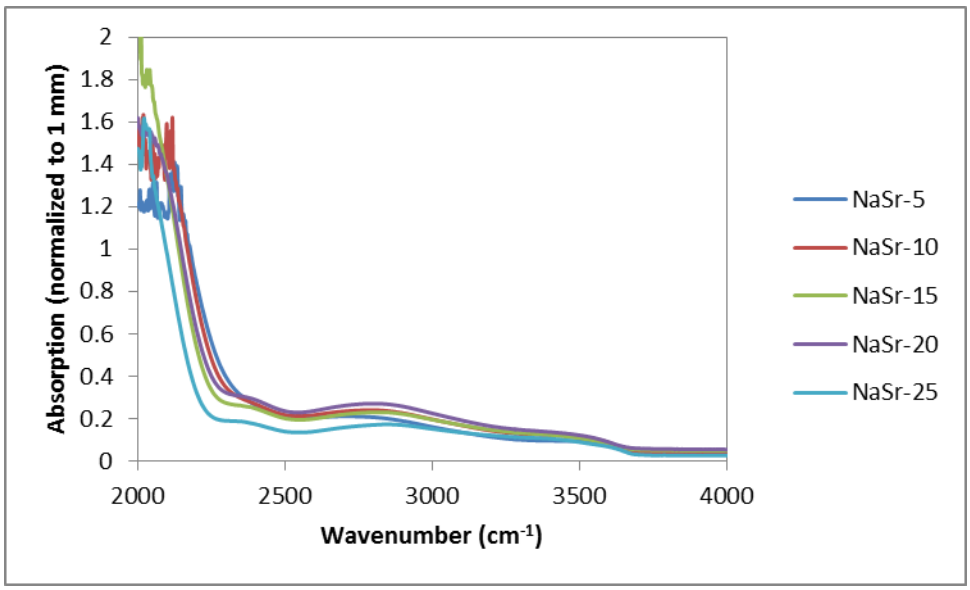

Figure 19. Fourier Transform Infrared spectroscopy spectrum for sodium strontium silicate series with strontium as the variable modifier.

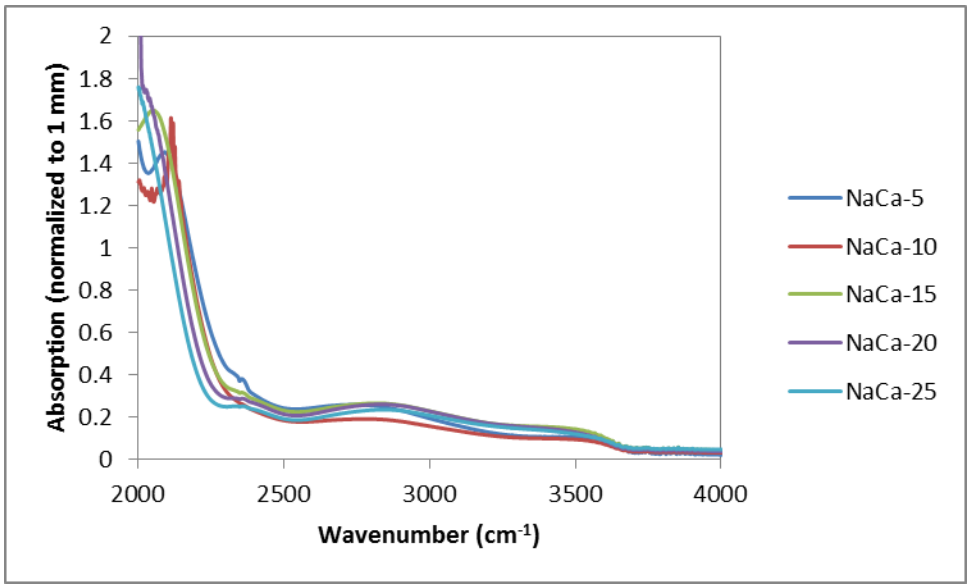

Figure 20. Fourier Transform Infrared spectroscopy spectrum for sodium calcium silicate series with calcium as the variable modifier.

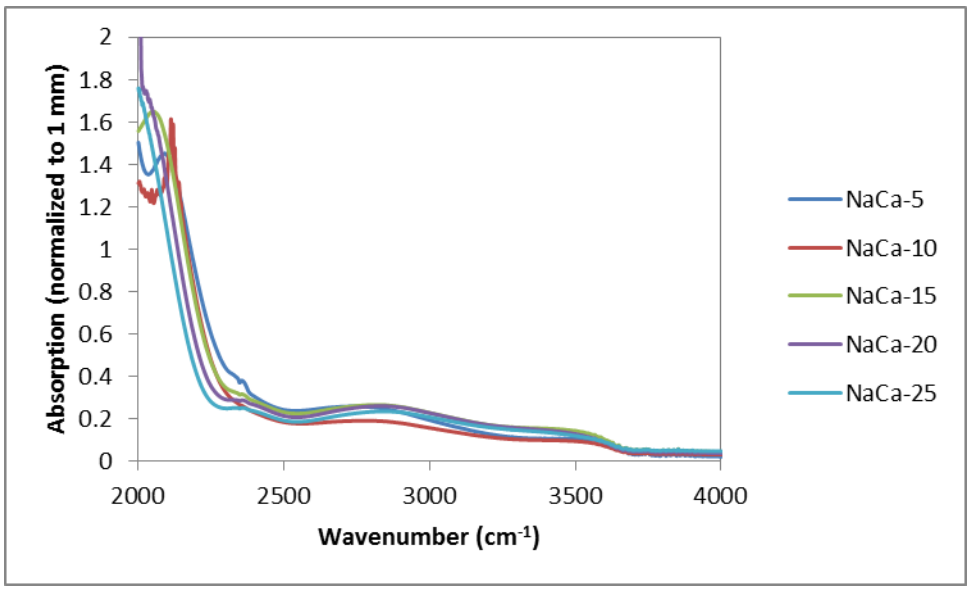

Figure 21. Fourier Transform Infrared spectroscopy spectrum for barium sodium silicate series with sodium as the variable modifier.

The second major feature presented in these figures is the multiphonon edge at the higher wavenumbers. This edge is the result of multiple absorptions from the many types of vibrational modes present in the glass structure. For these series of glasses there exists a general tendency to shift this edge towards longer wavenumbers with the addition of modifier. This relates back to the mass of the modifier ions and the bond strength.

F. Results and Discussion for Time-Domain Terahertz Spectropscopy

1. Compositional Effects

Figure 22, Figure 23, and Figure 24 shows the Absorption Coefficient as a function of frequency in the terahertz spectrum for variable barium, strontium, and calcium silicate respectively. The plots were Fourier Transformed from the time-domain to the frequency domain. In each of the figures there is little difference between the plots as a function of concentration as well for ion size. As for the plot shapes themselves the first feature to note is the slight rise in absorption near 0 THz. This is not a real phenomenon, and is a feature common in Terahertz spectroscopy as wavelengths at this frequency are blocked by the small sample holder, and thus appear as absorption. This

will be more evident in the dielectric plots in Figure 26, Figure 27, and Figure 28. In the frequency range of ~0.03-0.56 THz there is a rise in absorption, which is the result of the modifier ions absorption energies associated with vibrational modes.

This shows consistency with the properties of alkaline earth materials for this spectrum, and slight variances are the result of sample thickness differences, which are detailed in the third section of the Terahertz Results and Discussion.

It is known that pure fused silica has a minimal increase in absorption as the frequency increases and therefore the large increase in absorption must be a result of the additives within the glass, which is consistent with the results obtain by Naftaly and Miles.[35] In their study ionic polarizability of the modifiers increases the absorption coefficient with respect to frequency. From their conclusions the rate of increase depends on the glass type and modifiers present and chemical analysis was not correlated to the results. This means that the role of individual ion species has yet to be determined. From the results presented in Figure 22, Figure 23, and Figure 24 it is evident that the absorption is not strongly dependent on the concentration of alkaline ions as no significant difference exist in absorption plots of varying concentration.

There is also little difference in absorption coefficient due to ion size, which implies that using ions in the same group has little to no effect on the absorption coefficient. The glasses present in the study by Naftaly and Miles were commercial glasses with a variety of modifier types from multiple groups on the periodic table.[35] Some modifiers will interact non-linearly with other modifiers, but since the glass compositions are limited to only two modifiers at a time in this study, a mixed modifier effect still has yet to be explored.

The final feature of the plots presented in Figure 22, Figure 23, and Figure 24 are the leveling/extreme absorption of data series at the higher frequencies. This is a region of opacity and the actual absorption coefficient is too high to be a measureable value. This in turn invalidates any index of refraction/dielectric constant data that can be obtained. The different levels and the point where flat lining begins are dependent on the thickness of the sample.

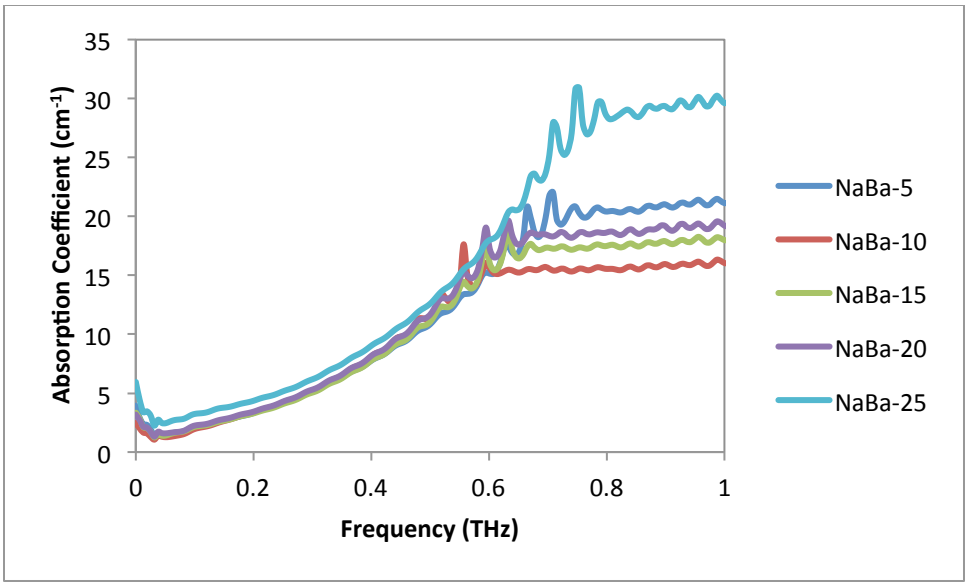

Figure 22. Absorption Coefficient as a function of Frequency in the Terahertz Spectrum for the sodium barium silicate series with barium as the variable modifier.

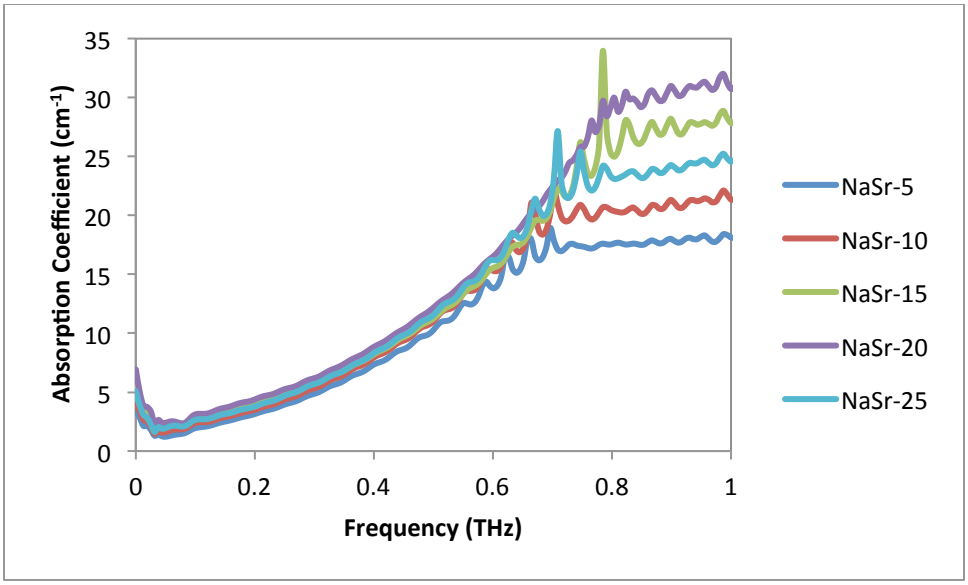

Figure 23. Absorption Coefficient as a function of Frequency in the Terahertz Spectrum for the sodium strontium silicate series with strontium as the variable modifier.

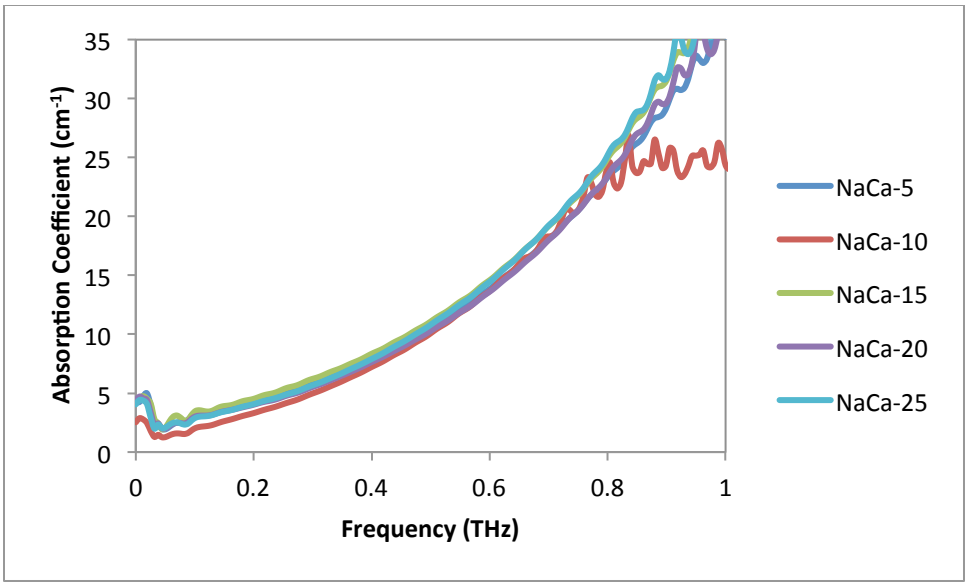

Figure 24. Absorption Coefficient as a function of Frequency in the Terahertz Spectrum for the sodium calcium silicate series with calcium as the variable modifier.

Figure 25 shows the Absorption coefficient as a function of frequency when sodium oxide is the variable modifier. This figure shows that increasing sodium content increases the absorption coefficient. This effect is less evident than was demonstrated in Figure 22, Figure 23, and Figure 24, but can be explained by the varying thickness of the glass scattering the terahertz radiation. The thinnest samples appear as the highest absorbing, as a result of more scattering.

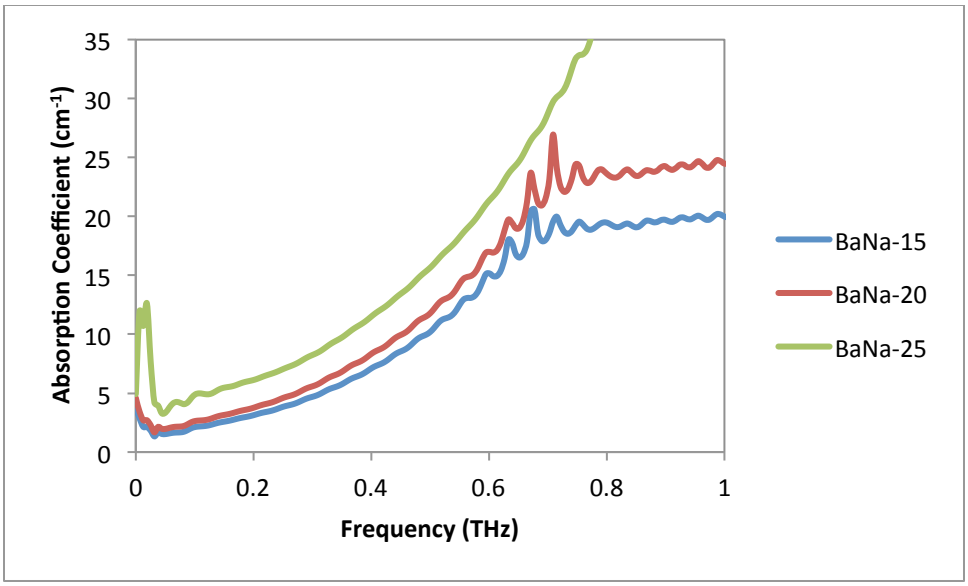

Figure 25. Absorption Coefficient as a function of Frequency in the Terahertz Spectrum for the barium sodium silicate series with sodium as the variable modifier.

Figure 26, Figure 27, and Figure 28 show the real and imaginary parts of the dielectric constant for variable concentrations of barium, strontium, and calcium respectively. In each of the figures the imaginary part is at a maximum (i.e. infinity) and the real part is at a minimum near 0 THz, which is due to the apparent opacity as described before. In the same region the increase in absorption coefficient, the real and imaginary parts of the dielectric constant can be calculated up to the point where no transmission occurs, which is around 0.6 THz. This is clearly marked by the sudden increase of a seemingly uniform dielectric constant. This other opaque region is attributed to multiphonon absorption. The same holds true in Figure 29 with variable sodium concentration where the dielectric constant also remains uniform for the region of adequate transmission.

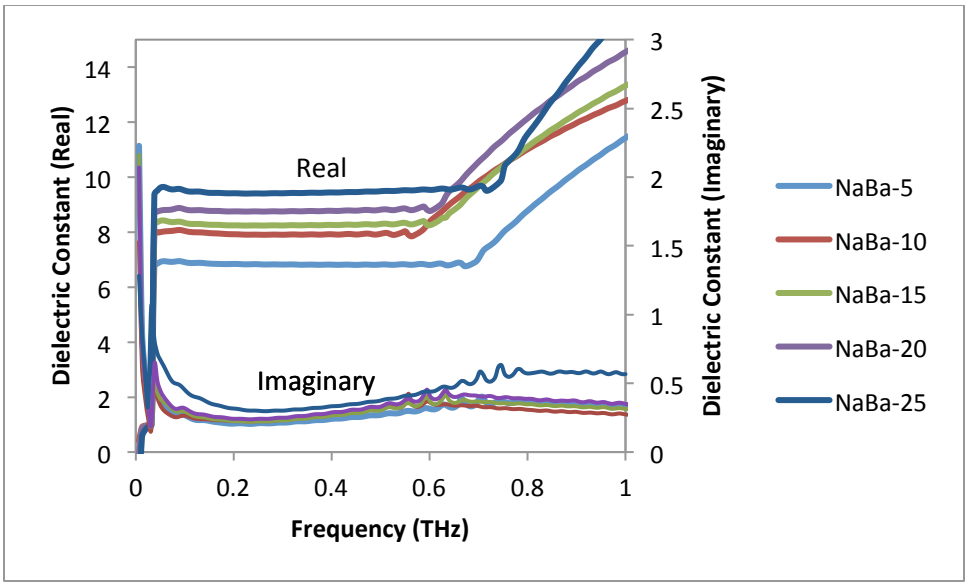

Figure 26. Real and Imaginary parts of the dielectric constant as a function of frequency in the Terahertz Spectrum for the sodium barium silicate series with barium as the variable modifier.

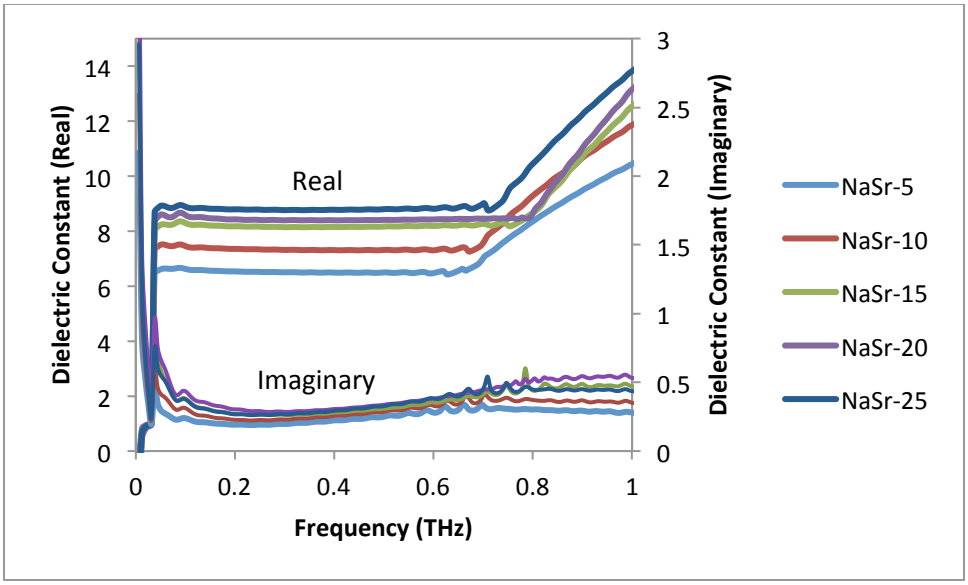

Figure 27. Real and Imaginary Parts of the dielectric constant as a function of frequency in the Terahertz Spectrum for the sodium strontium silicate series with strontium as the variable modifier.

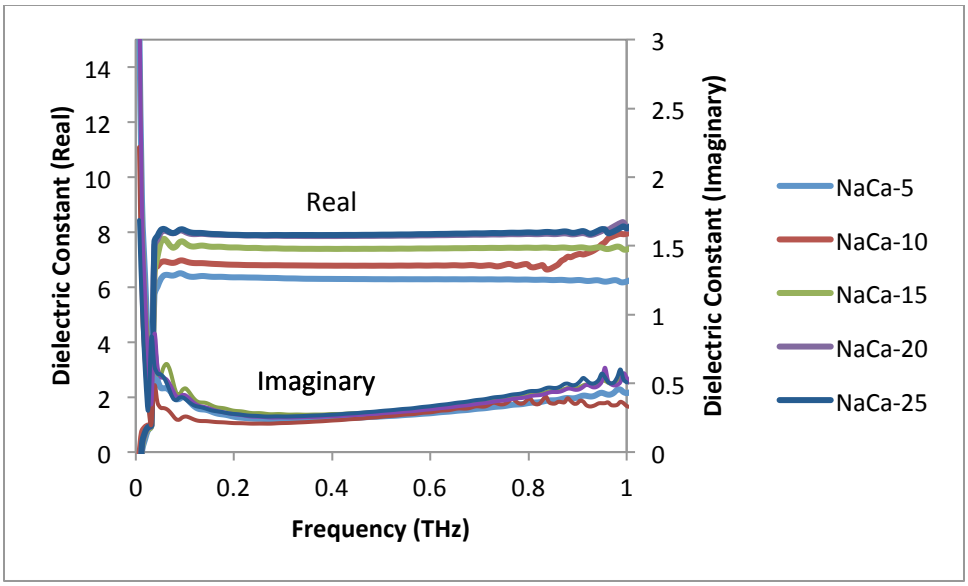

Figure 28. Real and Imaginary Parts of the dielectric constant as a function of Frequency in the Terahertz Spectrum for the sodium calcium silicate series with calcium as the variable modifier.

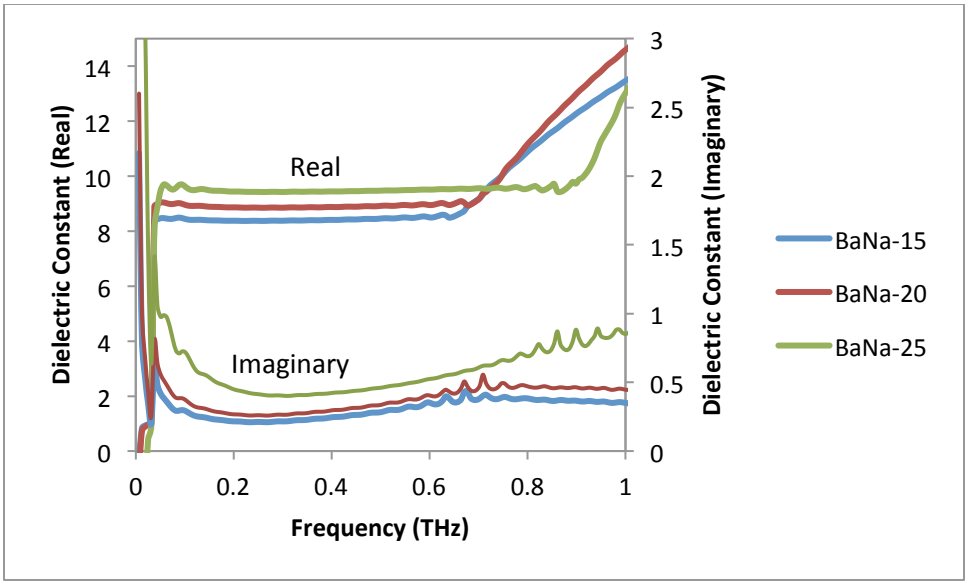

Figure 29. Real and Imaginary Parts of the dielectric constant as a function of Frequency in the Terahertz Spectrum for the barium sodium silicate series with sodium as the variable modifier.

To compare the series the dielectric constant was averaged in the region 0.050635 to 0.405077 THz and plotted as a function of the modifier additive, which is shown in

Figure 30. This region of the spectrum was chosen because there is transmission in all the tests performed. As shown in the plot the dielectric constant increases linearly as the concentration of modifier increases. It is also shown that as ion size increases so does the dielectric constant. The BaNa series seems to overlap the NaBa series. The similarity in composition between these two series is the reason for the overlay. Three possible explanations for the increase in dielectric constant exist: 1) The ionic polarizing nature of individual ion species with surrounding ions, 2) The addition of modifier lowers the density of the structure to allow for electron clouds to shift, and 3) The addition of modifier increase the amount of polarizing ions, which causes an apparent higher dielectric constant for the bulk glass. More realistically a combination of these three causes is reasonable.

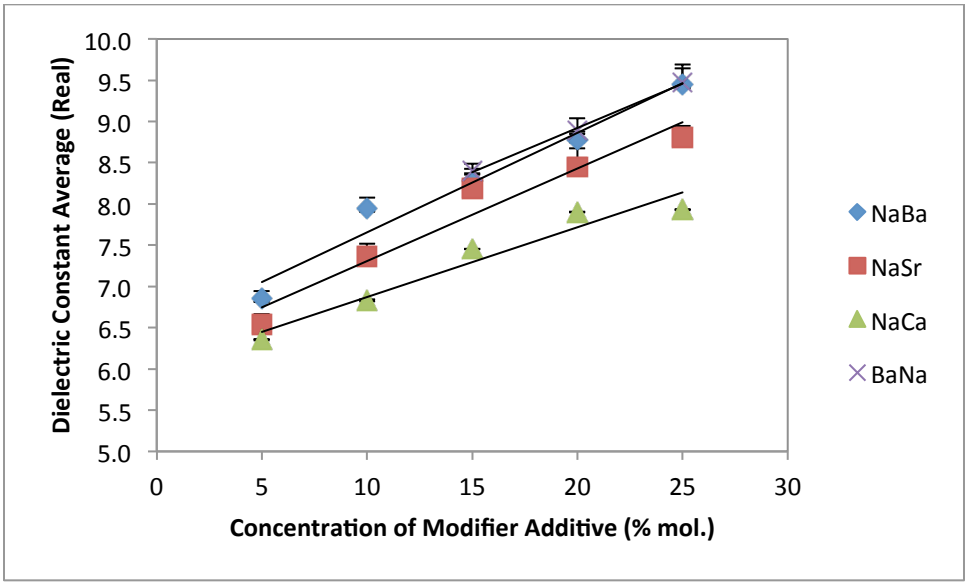

Figure 30. Dielectric constant average as a function of modifier type and concentration for all series.

A more open structure would also have an apparent change in density, as stated previously in the density results and discussion the density of each glass series increases with increasing modifier concentration. Figure 31 shows the dielectric constant as a function of density instead of modifier concentration. This plot shows that the dielectric constant is linearly dependent on the density. The slope of the dielectric constant

increases with decreasing modifier ionic size, but the dielectric constant is greater for glasses with larger modifier ionic size when concentration remains constant. For example at 5% mol RO (where R is Ba, Sr, or Ca) the average dielectric constant increases in the order Ba > Sr > Ca, which is in the order of decreasing field strength. In this figure the more vertical the trend lines are, the more likely that dielectric constant increase is due to the electronic polarization of the ionic species, and less on the local space (ionic polarization) surrounding polarizing ions. It is evident from this figure that all three reasons contribute to the dielectric constant increase because none of the series is completely vertical and thus the structure change must have an effect, though the sodium oxide varying series (BaNa) is near linear, which states that sodium ion concentration has a strong effect on the overall dielectric constant.

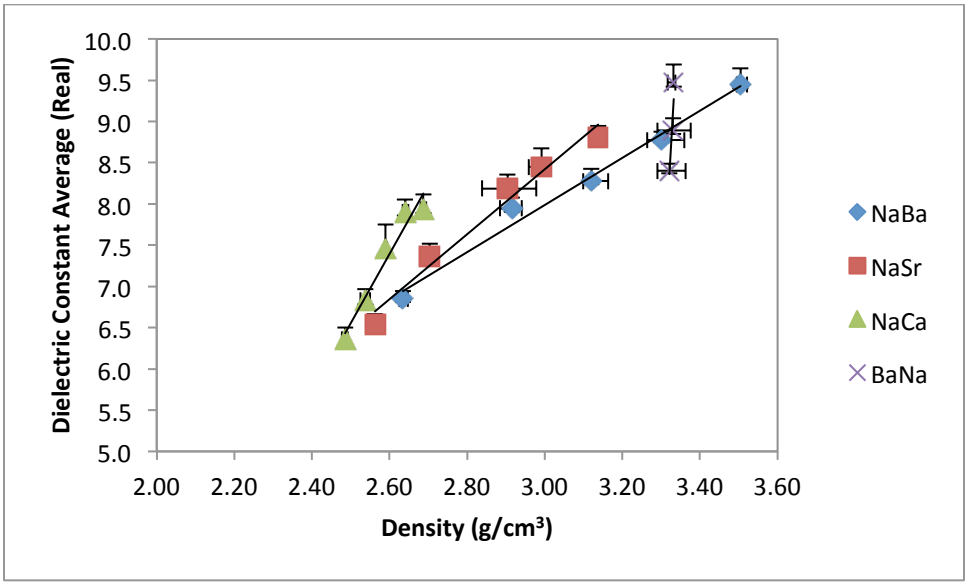

Figure 31. Dielectric constant average as a function of modifier type and density for all series.

2. Alternative Method of Testing

Figure 32 and Figure 33 shows the Transmission and Normalized Absorption respectively for glass frit in pellets that was produced in three quenching environments: Annealed (AN), Air Quenched (AQ) and Water Quenched (WQ). The composition used

for this study was chosen to be 20 Na_2O-15 BaO-60 SiO_2 and the sample powder was created from the same melt with the three different quenching methods. The goal was to quench the glass melt at a faster rate to change the density/glass transition temperature which directly relates to the structure. Table XII shows the density and glass transition temperature for each of these glasses where as the quenching rate increases, density decreases and glass transition temperature increases. From the figures there is no correlation that exists between the density vs. the transmission or absorption.

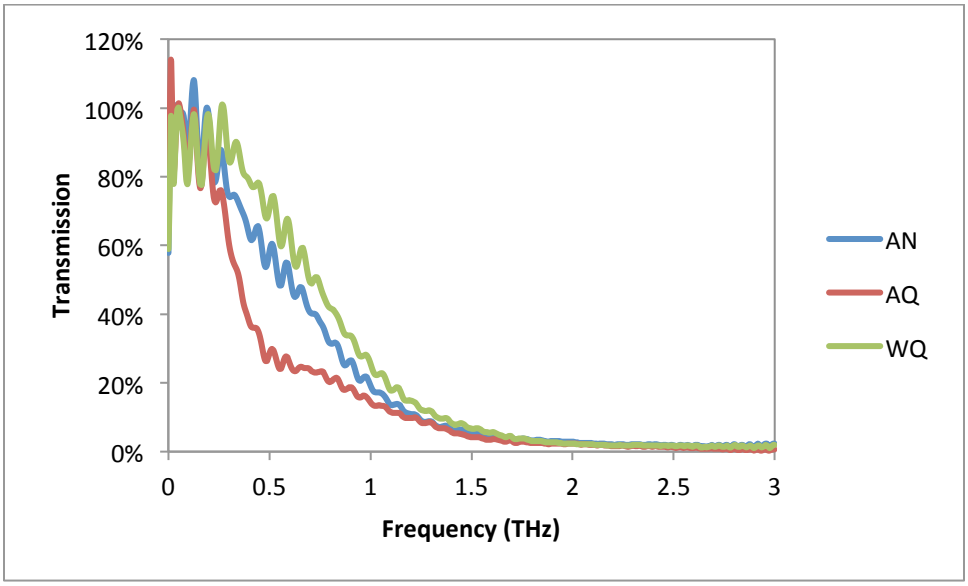

Figure 32. Transmission as a function of frequency in the Terahertz Spectrum for various quenched methods.

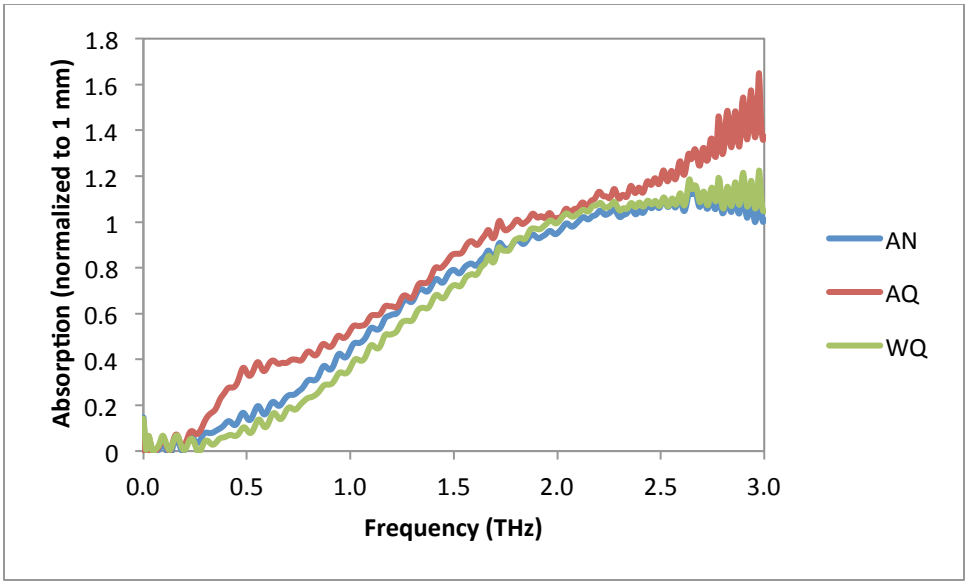

Figure 33. Absorption as a function of frequency in the Terahertz Spectrum for various quenched methods.

Table XII. Properties of the Glasses Prepared Using Different Quench Methods

Quench Method	Density (g/cm^3)	T_g (°C)
Annealed	3.1577	461
Air Quenched (AQ)	3.1332	464
Water Quenched (WQ)	3.0385	468

In Table XIII the mass of each of the components in the pellets, with the final mass of the pellets, and thickness dimensions was used to calculate the amount of frit per unit thickness (in this case 1 mm) in each of the samples when you assume complete homogeneity of frit to HDPE. It is a way of calculating the amount of frit in the HDPE for a given thickness, which is used to show how much frit is observed by the spectrometer. It is evident that even usual variances in measurements have significant effects on the transmission and apparent absorption. Using frit creates a large source of error with regards to the increased surface area and thus scattering effect of the radiation. From these results the proposed alternative method is deemed non-appropriate for glass analysis.

Table XIII. Sample Information for Pellets using different Quench Methods

Sample	HDPE wt. (mg)	NaBa-T wt. (mg)	Sample Mass (mg)	Sample Thickness (mm)	Frit (mg)	Frit (mg/mm)
Reference	360.1	0	327.7	1.458	-	-
AN	360.1	89.9	422.1	1.616	105.4	65.2
AQ	360	90	418.8	1.597	104.7	65.6
WQ	359.9	90.1	420.8	1.625	105.3	64.8

3. Ion Exchange/Thickness Effects

Figure 34 shows the transmission of a glass with the same composition, but with different thickness. The thickness of each sample is 2.204 mm and 3.239 mm for the thin and thick samples, respectively. At frequencies below 0.09 THz, the transmission remains similar regardless of the thickness. Above 0.09 THz the thick sample absorbs more of the THz radiation. For both plots the maximum transmission is about 56% at 0.044 THz for each sample. The drop in transmission between the thicknesses of the samples is clear that it is a factor in sample analysis. For dielectric constant and absorption coefficient, the thickness is used for calculating the values, but as seen before the absorption coefficient can be altered slightly by changing the sample thickness due to the wavelength being similar to the thickness causing scattering.

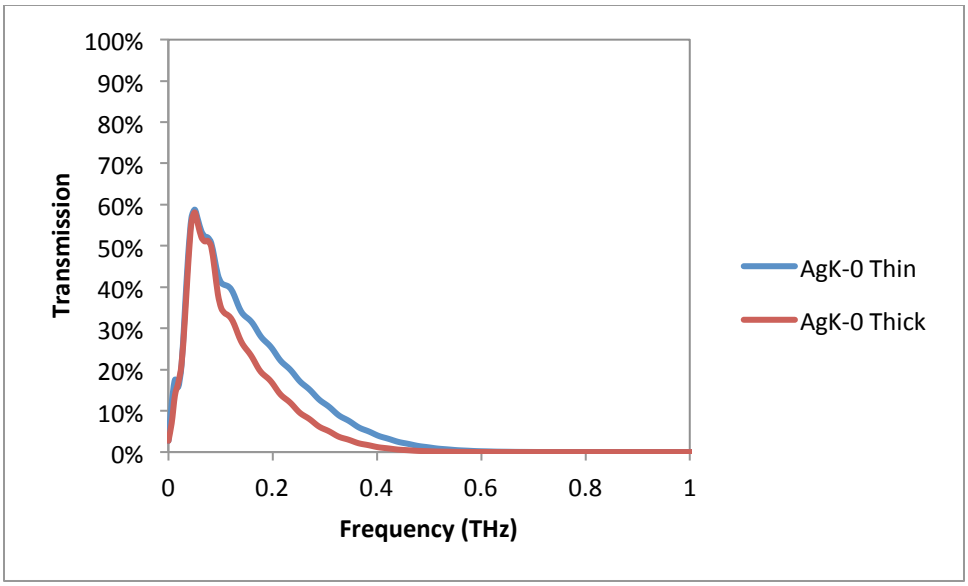

Figure 34. Transmission as a function of frequency in the Terahertz spectrum for a thin and thick commercial float glass.

Figure 35 shows the real and imaginary parts of the dielectric constant for two ion-exchanged samples with different heat treatment temperatures and an untreated sample. There is no difference when treated with silver or potassium in the terahertz spectrum. Figure 36 is the dielectric constant as a function of treatment temperature and it is clear no correlations exist. This lack of detection may be the result of the small layer of diffusion of the exchanged ions, which is on the order of 10's of microns, is too small for a response to the wavelengths in the terahertz spectrum, where 1 THz is equal to a wavelength of 300 microns.

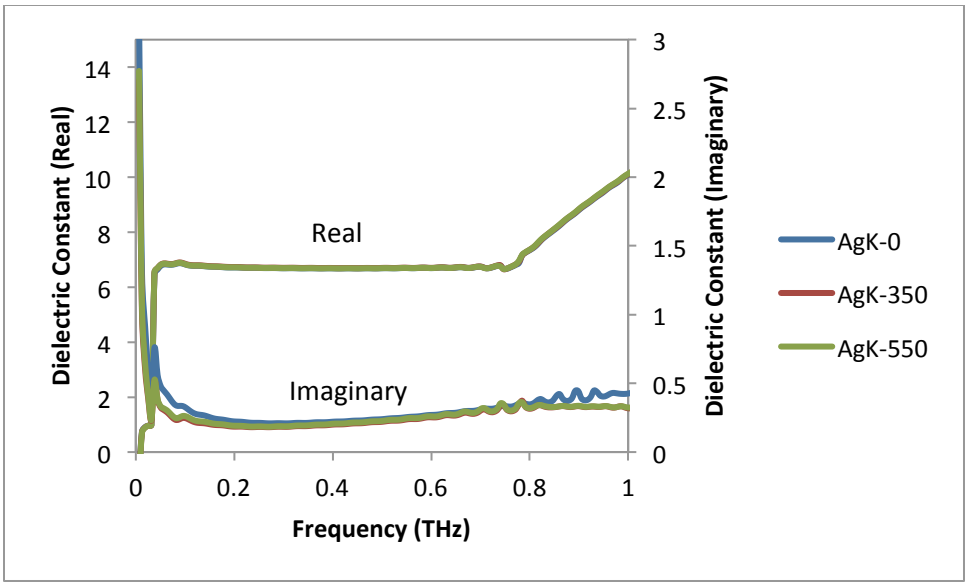

Figure 35. Real and Imaginary Parts of the dielectric constant as a function of Frequency in the Terahertz Spectrum for silver and potassium ion-diffused glass at various temperatures.

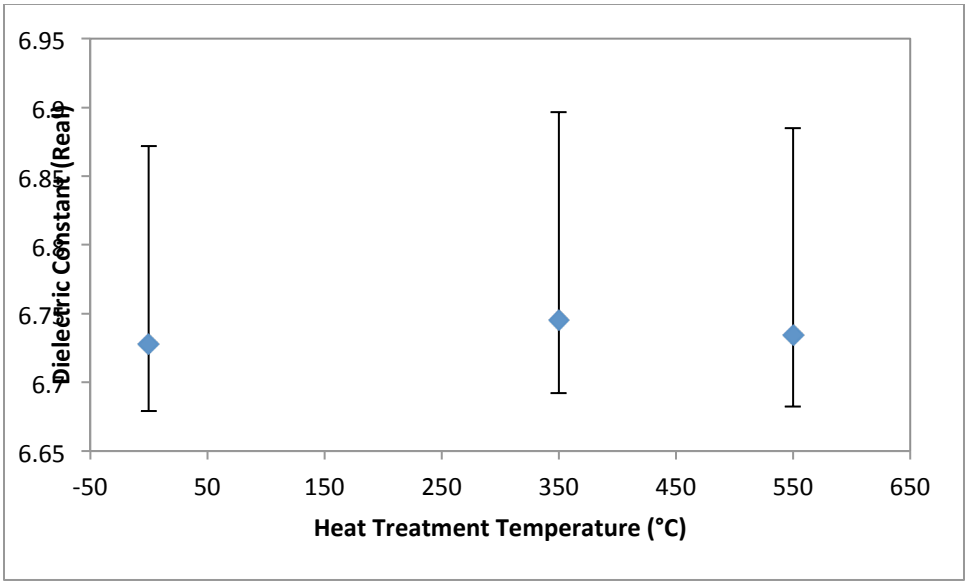

Figure 36. Dielectric constant average as a function of Heat Treatment Temperature for ion-diffused glasses.

4. Other Considerations for Terahertz Testing

Other factors which should be addressed are hydroxyl groups at the surface of the glasses, ambient temperature/atmosphere, data processing, surface reflection, and anion differences. Hydroxyl groups in the bulk of the glass as described previously have little effect on the data because to the absorption peaks of water vapor are not within the frequency range of measured data studied here, however, the presence of hydroxyl groups could affect data if the material is transparent at the rotational modes of water molecules bonded to the ions in the glass in the Terahertz region. From the testing in this study there appears to belittle effect from hydroxyl groups. There exist some absorption peaks in the Terahertz spectrum for water based molecules, but these peaks exist in the opaque domain region of the glass for this study, and therefore do not show up in the data.

This study was at room temperature, but an effect is theorized as it is known that glass will expand as temperature increases which alters the structure of the glass. The temperature during testing must be taken into consideration as the structure of glass will expand as temperature increases, and it is known that the density of glass has an effect on the dielectric constant.

The atmosphere does have an effect during data collection, especially due to water vapor in the air, but by purging the sample chamber with dry nitrogen these effects are greatly reduced. The atmosphere itself for this test is considered inert, but there are limited studies on the transparency of different gases.

The data processing can alter the results as well and it depends on the preference of the user as to which apodization method is used. As described in the introduction the same apodization, Blackmann-Harris 3-term, was applied to each series for consistency. Other Apodisation methods exist but the Blackmann-Harris 3-term method was considered a “best” choice. While the alteration results in only slight changes in the results, it still must be noted which method is used.

The surface reflection doesn’t show in the data presented but is apparent in the initial data of electric signal as a function of optical position. The reflection is a result of the index of refraction differences between the atmosphere and the glass. There also exist scattering from surface damage as a result of grinding and polishing. As stated in the

procedures, the glasses were polished to 1 μm, and at that level of polish there have been no major issues with the transmission of electromagnetic waves through the glasses. It is not to be completely ignored though as surface roughness will typically scatter light, but the terahertz wavelengths are much greater than the 1 μm polish.

For this study the cation effects in glass were studied, but the only anion present was oxygen. For other glasses where the anion is different from oxygen (e.g. fluorides, chalcogenides, metallic glasses, etc.), the field strength changes for ions and therefore an effect in the change in absorption coefficient as well as dielectric constant is theorized.

SUMMARY AND CONCLUSIONS

The significance of modifier selection will have a major impact on the electrical properties of glasses in the Terahertz region. The alkaline earth series will increase the dielectric constant as ion size increases in the group through ionic polarization. This increase in concentration of the modifier within the glass will also increase the dielectric constant as the increase in polarizing ions increases. Silicon replacement by the modifier ions are far more ionically polarizing and therefore increase the dielectric constant. Sodium particularly has a strong influence on the dielectric constant.

The dielectric constant increases for three reasons: The polarization nature of the ions present, the concentration of polarizing ions, and the free space availability locally surrounding the polarizing ions. The large ions are more easily electronically polarizable as the size of the electron clouds allows for more flexibility in movement. The large ions also open up the structure to allow for electron clouds to polarize more readily.

The open structure/density changes from thermal history cannot be characterized with the Terahertz Spectrometer using the alternative method described by the manufacturer. It is clear that the scattering effects are too high for an accurate measurement.

Thickness has an effect on the absorption of Terahertz light, and is not fully transparent. This indicates that there is scattering as a function of path length, and data must be normalized to a certain thickness for comparison.

Ion diffusivity of silver and potassium at the surface has no effect on the transmission or the dielectric constant in the Terahertz region. Terahertz radiation is too low energy to invoke a response to the silver and potassium ions, and silver ions are too far apart to be considered a metalized surface.

Hydroxyl groups at the surface of the glass can be neglected due to the opaque nature of glass at any water absorption frequencies in the Terahertz region. This holds true for oxide based glasses, and cannot carry over to other glasses that are based on other anions since the field strength changes.

FUTURE WORK

A wide range of materials still have yet to be explored within the Terahertz frequency region of the electromagnetic spectrum. This study focused on ion size as a glass modifier for one type of glass system. Numerous other glass systems i.e. gertmanates, chalcogenides, fluorides, phosphates, borates, etc. are still of interest as well as mixtures of these glass formers as well (e.g. borosilicates). Also the use of intermediates and other modifiers open up potential for future research as well. Still yet to be explored is the mixed alkali effect on glasses, and the glass-ceramic systems.

It is probably best to approach these future glasses from a glass structure point of view, meaning what effects the short and medium range order of the glasses? This can be characterized by X-Ray Diffraction and density, and more care should be given to correlate these effects. Thermal history, processing methods, storage environment, composition, size, geometry, testing conditions (heating/cooling, gas, electric/magnetic field) all leave future work open-ended with a variety of options. Since Terahertz Spectroscopy is a new field, the applications that link optics and electronics together still remain unexplored.

REFERENCES

1. M. Cooke, "Filling the THz Gap with New Applications," *Semicond. Today,* **2** [1] 39-43 (2007).

2. K. Kobayashi, "Thermogravimetric and MOS Capacitor Properties for PbO-Bi_2O_3-B_2O_3-SiO_2 Glass System," *J. Non-Cryst. Solids,* **124** [2–3] 229-32 (1990).

3. H. Tsuyuki, TDK Corporation, "Glass, Dielectric Composition, Multilayer Wiring Substrate, and Multilayer Ceramic Capacitor," US Pat. 5378662A, Jan., 1995.

4. A. Herezog and S. Stookey, "Glass and Methods of Devitrifying Same and Making a Capacitor Thereform," US Pat. 3195030, July, 1965.

5. C.J. Leedecke, N.G. Masse, M.J. Pryor, and N.N. Singhdeo, "Method of Manufacturing Glass Capacitors and Resulting Product," US Pat. 4687540, Aug., Aug. 1987.

6. C.E. Hutchins, E.W. Kuzia, P.M. Schmidt, and W.W. Schroeder, Sprague Electric Company, "Hermetically Sealed Aluminum Electrolytic Capacitor," US Pat. 4987519, Jan., 1991.

7. M. Koch, "Terahertz Communications: A 2020 Vision," 325-38 in NATO Security through Science Series, Vol. 19, *Terahertz Frequency Detection and Identification of Materials and Objects.* Edited by R. Miles, X.-C. Zhang, H. Eisele, and A. Krotkus. Springer, Netherlands, 2007.

8. P.Y. Han, M. Tani, M. Usami, S. Kono, R. Kersting, and X.C. Zhang, "A Direct Comparison between Terahertz Time-Domain Spectroscopy and Far-Infrared Fourier Transform Spectroscopy," *J. Appl. Phys.,* **89** [4] 2357-9 (2001).

9. C.A. Schmuttenmaer, "Exploring Dynamics in the Far-Infrared with Terahertz Spectroscopy," *Chem. Rev.,* **35** [24] 1759-79 (2004).

10. I. Pupeza, R. Wilk, and M. Koch, "Highly Accurate Optical Material Parameter Determination with THz Time-Domain Spectroscopy," *Opt. Express,* **15** [7] 4335-50 (2007).

11. L. Solymar and D. Walsh, *Electrical Properties of Materials,* 8th ed. Oxford University Press, Oxford, UK, 2010.

12. P.D. Cunningham, "Optical Pump Terahertz Probe Studies of Semiconducting Polymers"; Ph.D. Thesis. University of Maryland, Baltimore County, 2010.

13. J. Chen, Y. Chen, H. Zhao, G.J. Bastiaans, and X.C. Zhang, "Absorption Coefficients of Selected Explosives and Related Compounds in the Range of 0.1-2.8 THz," *Opt. Express,* **15** [19] 12060 7pp. (2007).

14. E.P.J. Parrott, J.A. Zeitler, T. Friscic, M. Pepper, W. Jones, G.M. Day, and L.F. Gladden, "Testing the Sensitivity of Terahertz Spectroscopy to Changes in Molecular and Supramolecular Structure: A Study of Structurally Similar Cocrystals," *Cryst. Growth Des.,* **9** [3] 1452-60 (2009).

15. S. Wietzke, C. Jansen, T. Jung, M. Reuter, B. Baudrit, M. Bastian, S. Chatterjee, and M. Koch, "Terahertz Time-Domain Spectroscopy as a Tool to Monitor the Glass Transition in Polymers," *Opt. Express,* **17** [21] 19006-14 (2009).

16. P. Jepsen, H. Merbold, Z. Li, X. Xing, and S. Clark, "Terahertz Time-Domain Spectroscopy of Crystalline and Aqueous Systems," 147-65 in NATO Security through Science Series, Vol. 19, *Terahertz Frequency Detection and Identification of Materials and Objects.* Edited by R. Miles, X.-C. Zhang, H. Eisele, and A. Krotkus. Springer, Netherlands, 2007.

17. S. van der Gijp, "Preparation of Homogeneously-Doped Barium Titanate"; Ph.D. Thesis. Universiteit Twente, Enschede, Netherland, 1998.

18. H. Jiawang, G. Catalan, J.F. Scott, and E. Artacho, "The Flexoelectricity of Barium and Strontium Titanates from First Principles," *J. Phys.: Condens. Matter,* **22** [11] 112201 6pp. (2010).

19. F. Moura, A.Z. Simões, B.D. Stojanovic, M.A. Zaghete, E. Longo, and J.A. Varela, "Dielectric and Ferroelectric Characteristics of Barium Zirconate Titanate Ceramics Prepared from Mixed Oxide Method," *J. Alloys Compd.,* **462** [1–2] 129-34 (2008).

20. H.Y. Tian, Y. Wang, J. Miao, H.L.W. Chan, and C.L. Choy, "Preparation and Characterization of Hafnium Doped Barium Titanate Ceramics," *J. Alloys Compd.,* **431** [1–2] 197-202 (2007).

21. C.-H. Kim, K.-J. Park, Y.-J. Toon, Y.-T. Kim, and K.-H. Hur, "Formation of Core-Shell Structure in $BaTiO_3$ Grains," *J. Korean Ceram. Soc.,* **46** [2] 123-30 (2009).

22. M.-N. Lee and Y.-C. Park, "Dielectric Properties and an EPR Study of Cu-or Zr-Doped $BaTiO_3$ Ceramics," *Bull. Korean Chem. Soc.,* **16** [10] 908-11 (1995).

23. C.M. Randall and R.D. Rawcliffe, "Refractive Indices of Germanium, Silicon, and Fused Quartz in the Far Infrared," *Appl. Opt.,* **6** [11] 1889-95 (1967).

24. W.F. Passchier, D.D. Honijk, M. Mandel, and M.N. Afsar, "A New Method for the Determination of Complex Refractive Index Spectra of Transparent Solids in the Far-Infrared Spectral Region: Results of Pure Silicon and Crystal Quartz," *J. Phys. D: Appl. Phys.,* **10** [4] 509-17 (1977).

25. E.V. Loewenstein, D.R. Smith, and R.L. Morgan, "Optical Constants of Far Infrared Materials. 2: Crystalline Solids," *Appl. Opt.,* **12** [2] 398-406 (1973).

26. M.N. Afsar, "Dielectric Measurements of Millimeter-Wave Materials," *Proc. IEEE,* **73** [1] 131-53 (1985).

27. A.K.W. Abdullah, K.A. Maslin, and T.J. Parker, "Observation of Two-Phonon Difference Bands in the FIR Transmission Spectrum of Si," *Infrared Phys.,* **24** [2–3] 185-8 (1984).

28. J.R. Birch, "The Absolute Determination of Complex Reflectivity," *Infrared Phys.,* **18** [5–6] 613-20 (1978).

29. D. Grischkowsky, S. Keiding, M.v. Exter, and C. Fattinger, "Far-Infrared Time-Domain Spectroscopy with Terahertz Beams of Dielectrics and Semiconductors," *J. Opt. Soc. Am. B,* **7** [10] 2006-15 (1990).

30. M. Naftaly and R. Dudley, "Terahertz Reflectivities of Metal-Coated Mirrors," *Appl. Opt.,* **50** [19] 3201-4 (2011).

31. S. Kojima, H. Kitahara, S. Nishizawa, Y.S. Yang, and M. Wada Takeda, "Terahertz Time-Domain Spectroscopy of Low-Energy Excitations in Glasses," *J. Mol. Struct.,* **744–747** 243-6 (2005).

32. S. Kojima, M. Wada Takeda, and S. Nishizawa, "Terahertz Time Domain Spectroscopy of Complex Dielectric Constants of Boson Peaks," *J. Mol. Struct.,* **651–653** 285-8 (2003).

33. M. Naftaly and R. Miles, "Terahertz Beam Interactions with Amorphous Materials," 107-22 in NATO Security through Science Series, Vol. 19, *Terahertz Frequency Detection and Identification of Materials and Objects.* Edited by R. Miles, X.-C. Zhang, H. Eisele, and A. Krotkus. Springer, Netherlands, 2007.

34. M. Naftaly and R.E. Miles, "Terahertz Time-Domain Spectroscopy: A New Tool for the Study of Glasses in the Far Infrared," *J. Non-Cryst. Solids,* **351** [40–42] 3341-6 (2005).

35. M. Naftaly and R.E. Miles, "Terahertz Time-Domain Spectroscopy of Silicate Glasses and the Relationship to Material Properties," *J. Appl. Phys.,* **102** [4] 043517 6pp. (2007).

36. E.P.J. Parrott, J.A. Zeitler, L.F. Gladden, S.N. Taraskin, and S.R. Elliott, "Extracting Accurate Optical Parameters from Glasses Using Terahertz Time-Domain Spectroscopy," *J. Non-Cryst. Solids,* **355** [37–42] 1824-7 (2009).

37. E.P.J. Parrott, J.A. Zeitler, G. Simon, B. Hehlen, L.F. Gladden, S.N. Taraskin, and S.R. Elliott, "Atomic Charge Distribution in Sodosilicate Glasses from Terahertz Time-Domain Spectroscopy," *Phys. Rev. B,* **82** [14] 140203 4pp. (2010).

38. S.N. Taraskin, S.I. Simdyankin, and S.R. Elliott, "The Atomic Charge Distribution in Glasses Obtained by Terahertz Spectroscopy," *J. Phys.: Condens. Matter,* **19** [45] 455216 7pp. (2007).

39. J.E. Shelby, *Introduction to Glass Science and Technology,* 2nd ed. The Royal Society of Chemistry, Cambridge, UK, 2005.

40. T. Izumitani and H. Toratani, "Temperature Coefficient of Electronic Polarizability in Optical Glasses," *J. Non-Cryst. Solids,* **40** [1–3] 611-9 (1980).

41. V. Dimitrov and T. Komatsu, "Classification of Oxide Glasses: A Polarizability Approach," *J. Solid State Chem.,* **178** [3] 831-46 (2005).

42. G.D. Quinn, "Fractography of Ceramics and Glasses" (2007) NIST. Accessed on: Jan. 25, 2012. Available at <http://www.nist.gov/customcf/get_pdf.cfm?pub_id=850928>

43. H. Coker, "The Electronic Strain Polarizability Constants of the Alkali Halides," *J. Phys. Chem. Solids,* **40** [12] 1079-88 (1979).

44. C.Z. Tan and J. Arndt, "The Mean Polarizability and Density of Glasses," *Phys. B: Condens. Matter,* **229** [3–4] 217-24 (1997).

45. C.C. Homes, T. Vogt, S.M. Shapiro, S. Wakimoto, and A.P. Ramirez, "Optical Response of High-Dielectric-Constant Perovskite-Related Oxide," *Science,* **293** [5530] 673-6 (2001).

46. M. Fox, *Optical Properties of Solids,* 2nd ed. Oxford University Press, Oxford, U.K., 2010.

47. N.A. Sharaf, R.A. Condrate Sr, and A.A. Ahmed, "FTIR Spectral/Structural Investigation of the Ion Exchange/Thermal Treatment of Silver Ions into a Silicate Glass," *Mater. Lett.,* **11** [3–4] 115-8 (1991).

48. H. Wakabayashi and M. Tomozawa, "Diffusion of Water into Silica Glass at Low Temperature," *J. Am. Ceram. Soc.,* **72** [10] 1850-5 (1989).

49. T.T. Chen, J.E. Dutrizac, K.E. Haque, W. Wyslouzil, and S. Kashyap, "The Relative Transparency of Minerals to Microwave Radiation," *Can. Metall. Q.,* **23** [3] 349-51 (1984).

50. N.N. Singhdeo, M.J. Pryor, C.J. Leedecke, and N.G. Masse, Olin Corporation, "Method of Manufacturing Glass Capacitors and Resulting Product," US Pat. 4,687,540, Aug., 1987.

51. B. Rangarajan, B. Jones, T. Shrout, and M. Lanagan, "Barium/Lead-Rich High Permittivity Glass–Ceramics for Capacitor Applications," *J. Am. Ceram. Soc.,* **90** [3] 784-8 (2007).

52. N.P. Bansal and R.H. Doremus, *Handbook of Glass Properties*. Academic Press, Orlando, FL, 1986.

53. A. Paul, "Chemical Durability of Glasses; a Thermodynamic Approach," *J. Mater. Sci.,* **12** [11] 2246-68 (1977).

54. G. Stewart, C.A. Millar, P.J.R. Laybourn, C.D.W. Wilkinson, and R. DelaRue, "Planar Optical Waveguides Formed by Silver-Ion Migration in Glass," *IEEE J. Quantum Electron.,* **13** [4] 192-200 (1977).

55. R.H. Doremus, "Exchange and Diffusion of Ions in Glass," *J. Phys. Chem.,* **68** [8] 2212-8 (1964).

56. G.W. Arnold and J.A. Borders, "Aggregation and Migration of Ion-Implanted Silver in Lithia-Alumina-Silica Glass," *J. Appl. Phys.,* **48** [4] 1488-96 (1977).

57. R.V. Ramaswamy and R. Srivastava, "Ion-Exchanged Glass Waveguides: A Review," *J. Lightwave Technol.,* **6** [6] 984-1000 (1988).

58. R. Shannon, "Revised Effective Ionic Radii and Systematic Studies of Interatomic Distances in Halides and Chalcogenides," *Acta Crystallogr., Sect. A,* **32** [5] 751-67 (1976).

59. L. De Ferri, D. Bersani, A. Lorenzi, P.P. Lottici, G. Vezzalini, and G. Simon, "Structural and Vibrational Characterization of Medieval Like Glass Samples," *J. Non-Cryst. Solids,* **358** [4] 814-9 (2012).

60. J. Göttlicher, H.J. Pentinghaus, and B. Himmel, "On the Microstructure of Geyserites and Hyalites, Natural Hydrous Forms of Silica," *J. Sol-Gel Sci. Technol.,* **13** [1-3] 85-8 (1998).

61. J. Swenson and L. Börjesson, "Intermediate Range Ordering in a Network Glass," *J. Non-Cryst. Solids,* **223** [3] 223-9 (1998).

62. M. Akira, K. Shinji, and U. Takashi, "Modification of Medium-Range Order in Silica Glass by Ball-Milling: Real- and Reciprocal-Space Structural Correlations for the First Sharp Diffraction Peak," *J. Phys.: Condens. Matter,* **19** [45] 455214 7pp. (2007).

63. E.A.P. De Maeyer and R.M.H. Verbeeck, "X-Ray Diffraction Study of Acid-Degradable Glasses," *J. Dent. Res.,* **80** [8] 1764-7 (2001).

64. A. Fluegel, "Modeling of Glass Liquidus Temperatures Using Disconnected Peak Functions," S1-2 in *Proceedings of the 2007 ACerS Glass & Optical Materials Division Meeting & 18th University Conference on Glass.* Edited by M. Hall and C. Click. American Ceramic Society, Westerville, OH, 2007. CD-ROM.

65. F.A. Moustaffa, F.H. El-Batal, A.M. Fayadd, and I.M. El-Kashef, "Absorption Studies on Some Silicate and Cabal Glasses Containing NiO or Fe_2O_3 or Mixed NiO + Fe_2O_3," *Acta Phys. Pol., A,* **117** [3] 471-7 (2010).

66. A.M. Efimov and V.G. Pogareva, "Water-Related IR Absorption Spectra for Some Phosphate and Silicate Glasses," *J. Non-Cryst. Solids,* **275** [3] 189-98 (2000).

67. A.M. Efimov, V.G. Pogareva, and A.V. Shashkin, "Water-Related Bands in the IR Absorption Spectra of Silicate Glasses," *J. Non-Cryst. Solids,* **332** [1–3] 93-114 (2003).